

**THE HYPABYSSAL 5034 KIMBERLITE OF THE GAHCHO KUE CLUSTER,  
SOUTHEASTERN SLAVE CRATON, NORTHWEST TERRITORIES, CANADA:  
A GRANITE-CONTAMINATED GROUP-I KIMBERLITE**

GUILLAUME CARO<sup>¶</sup> AND MAYA G. KOPYLOVA<sup>§</sup>

*Department of Earth and Ocean Sciences, The University of British Columbia, 6339 Stores Road,  
Vancouver, British Columbia V6T 1Z4, Canada*

ROBERT A. CREASER

*Department of Earth and Atmospheric Sciences, University of Alberta, Edmonton, Alberta T6G 2E3, Canada*

ABSTRACT

We present petrographic, mineralogical, geochemical and isotopic data on the 5034 kimberlite of the Cambrian Gahcho Kue kimberlite cluster (Slave craton, northern Canada). This Group-IA kimberlite is a multiphase intrusion composed of the diatremefacies magmatic and hypabyssal kimberlite, which intruded in at least four magmatic phases. The dominant hypabyssal phase is composed of macrocrystal monticellite – phlogopite – serpentine kimberlite. Occasional samples with diopside ± melilite may reflect local heterogeneities in the bulk composition or separate intrusive phases. Aphanitic monticellite – serpentine kimberlite forms as early and contemporaneous small-volume magmas and is present in autoliths and in cross-cutting dykes. The subsequent explosive magmatic phase formed tuffisitic kimberlite breccia, which in turn is cut by macrocrystal phlogopite – serpentine kimberlite. The phlogopite in all recognized hypabyssal rock-types has distinct compositional trends, but within a given rock-type, it also varies significantly in response to local chemical heterogeneities and to the composition of minerals adjacent to it. The large variability in phlogopite compositions is due to very local diffusion-controlled crystallization, and not to changes in bulk composition of the magma. All varieties of the 5034 kimberlite show strong evidence of contamination by host granitic rocks. Pectolite, diopside, melilite and phlogopite have replaced and crystallized around partly assimilated granitic xenoliths from a hybrid melt enriched in Si and Na. A high activity of Si may be the major factor controlling the presence of melilite in kimberlites. The mineralogical character of the 5034 kimberlite, which is intermediate between Group-I and Group-II kimberlites, can be explained by its strong contamination by granites. The composition of the kimberlite in terms of Sr and Nd isotopes suggests an asthenospheric origin of the melt and allows for incorporation of no more than 8–12% granitic material into the parental magma.

*Keywords:* kimberlite, phlogopite, spinel, Sr and Nd isotopes, granite contamination, melilite, Slave craton, Gahcho Kue cluster, Northwest Territories, Canada.

SOMMAIRE

Nous présentons des données pétrographiques, minéralogiques, géochimiques et isotopiques à propos de la kimberlite 5034 de l'agglomération de kimberlites de Gahcho Kue (d'âge cambrien, craton de l'Esclave, partie nord du Canada). Cette kimberlite à affinités au groupe IA est une intrusion multiphasée composée de kimberlite ayant un faciès diatreme et de kimberlite subvolcanique, mise en place en au moins quatre venues. La phase subvolcanique dominante est composée de kimberlite à macrocristaux de monticellite – phlogopite – serpentine. Les échantillons contenant l'assemblage diopside ± mélilite, plutôt occasionnels, pourrait résulter d'hétérogénéités locales en composition du magma ou bien d'une venue intrusive séparée. La kimberlite aphanitique à monticellite – serpentine s'est formée de façon précoce à partir de petits volumes de magma kimberlitique et se présente sous forme d'autolithes et en filons tardifs. Vient ensuite une phase magmatique explosive qui a formé la kimberlite tuffisitique bréchique, et enfin une kimberlite à macrocristaux de phlogopite + serpentine. La composition de la phlogopite dans tous ces variantes subvolcaniques montre des tracés évolutifs distincts, mais au sein d'un type de roche, elle varie aussi selon les hétérogénéités locales et la composition des minéraux adjacents. La variabilité marquée de la composition de la phlogopite serait due à sa cristallisation régie très localement par la diffusion, et non aux changements en composition globale du magma. Toutes variétés de la kimberlite 5034 témoignent d'une contamination marquée par les roches-hôtes granitiques. Pectolite, diopside,

<sup>¶</sup> *Present address:* Géochimie – Cosmochimie (UMR 7579 CNRS), Institut de Physique du Globe de Paris, Université Denis Diderot, 4, place Jussieu, F-75252 Paris Cedex 05, France.

<sup>§</sup> *E-mail address:* mkopylov@eos.ubc.ca

mélilite et phlogopite ont remplacé et cristallisé autour de xénolithes granitiques partiellement assimilés à partir d'un magma hybride enrichi en Si et Na. Une activité accrue de Si pourrait bien être un facteur régissant la présence de mélilite dans ces kimberlites. Le caractère minéralogique de la kimberlite 5034, qui est intermédiaire entre les kimberlites de groupe I et ceux de groupe II, pourrait résulter d'une forte contamination par le granite. La composition de la kimberlite en termes des isotopes de Sr et de Nd indique une origine asthénosphérique et permet une incorporation d'au plus 8 à 12% de matériau granitique dans le magma parental.

(Traduit par la Rédaction)

*Mots-clés:* kimberlite, phlogopite, spinelle, isotopes de Sr et de Nd, contamination par matériau granitique, mélilite, craton de l'Esclave, agglomération de Gahcho Kue, Territoires du Nord-Ouest, Canada.

## INTRODUCTION

Our understanding of the petrology and geology of kimberlites has increased substantially as a result of new discoveries in Canada. Kimberlites are now found in all parts of northern Canada, from Coronation Bay in the west to Quebec in the east. In spite of the major surge in publications related to the 8<sup>th</sup> International Kimberlite Conference in Victoria in 2003, relatively little geological information on kimberlites is found in the public domain. Moreover, most publications on Canadian kimberlites focus on internal geology, facies and textures of the rocks (*e.g.*, Field & Scott Smith 1999, Hetman *et al.* 2003), and the authors do not report detailed mineralogical information. This work aims at filling these gaps.

We report petrographic, mineralogical, geochemical and isotopic data on the 5034 hypabyssal kimberlite of the Gahcho Kue kimberlite cluster, which is moderately diamondiferous. The geological content, textural varieties and kimberlite facies of this cluster make this one of the best understood kimberlites in the Slave craton, as it was a focus of extensive drilling and textural studies (Rikhotso *et al.* 2003, Hetman *et al.* 2003). This work complements the geological model of the Gahcho Kue kimberlites by providing geochemical and mineralogical data on a parent magmatic kimberlite that was explosively intruded, forming breccias.

This study is based on samples recovered from the large-diameter cores drilled in 1995–1997 by Canamera Ltd. (a contractor for Mountain Province Ltd.) for bulk sampling in the diamond-exploration program. Eleven representative samples of the fresher hypabyssal kimberlite were chosen for our detailed studies from the UBC collection of ~60 specimens of the 5034 kimberlite. We characterize the kimberlite through compositional data on the rock-forming minerals and whole rocks that form several magmatic phases. We show that many of its mineralogical and petrological traits can be explained by its strong contamination by granitic xenoliths. In this work, we also address the presence of melilite in kimberlites, the nomenclature and origin of kimberlites intermediate between Group I and Group II, the use of compositional trends in spinel and phlogopite for the systematics of kimberlites and related alkaline

rocks (Mitchell 1995), and the extent to which xenolithic material was incorporated into the kimberlitic magma.

## THE GAHCHO KUE KIMBERLITES

The Gahcho Kue cluster of kimberlites (Fig. 1) is located about 75 km south of Aylmer Lake in the southeastern corner of the Slave craton (63°30'N, 109°30'W), 280 km northeast of Yellowknife, in the Northwest Territories. Six bodies of kimberlite of the Gahcho Kue cluster (the 5034, 5034-South, Tesla, Tuzo, Hearn and Wallace, Fig. 1) may represent the oldest known occurrence of kimberlite on the Slave Craton. The 5034 kimberlite has been dated radiometrically by the Rb–Sr method on phlogopite as being Middle Cambrian (542.2 ± 2.6 Ma: Heaman *et al.* 2003).

The four main pipes, 5034, Hearne, Tuzo and Tesla, have contrasting external shapes and pipe infills; the latter are dominated by hypabyssal kimberlite (HK) and tuffisitic kimberlite breccia (TKB). There is a correlation between pipe shape and texture of the kimberlite infill. Tuffisitic kimberlite breccia occurs in the circular smooth-sided pipes, Tuzo and Hearne South, whereas hypabyssal kimberlite dominates the complex irregular pipe at 5034. At Hearne North and Tesla, intermediate shapes of pipes contain both TKB and HK, with a significant amount of kimberlite displaying textures that are gradational from TKB to HK materials with increasing depth. There is also a correlation between pipe shape and internal geology, ranging from simple to complex from Tuzo, through Tesla and Hearn, to 5034.

The 5034 pipe has an irregular shape, and a 35-m-wide dike-like body extends from the pipe some 300 m to the north-northeast (Fig. 2). The overall near-surface area is about 2.15 ha, and the majority of it is under Kennady Lake. The 5034 pipe was subdivided on the basis of internal geology into four lobes (Figs. 1, 2), a western, central, and eastern lobe, as well as a northern lobe intersected in drill core. The lobes differ in modeled diamond grade from 1.3 to 1.85 ct/t (The Mountain Province Diamonds Inc. Annual Report 2002).

In summary, the geology, shape and infill of the individual kimberlite pipes at Gahcho Kue are similar to those of the kimberlites in the Kimberley area of South

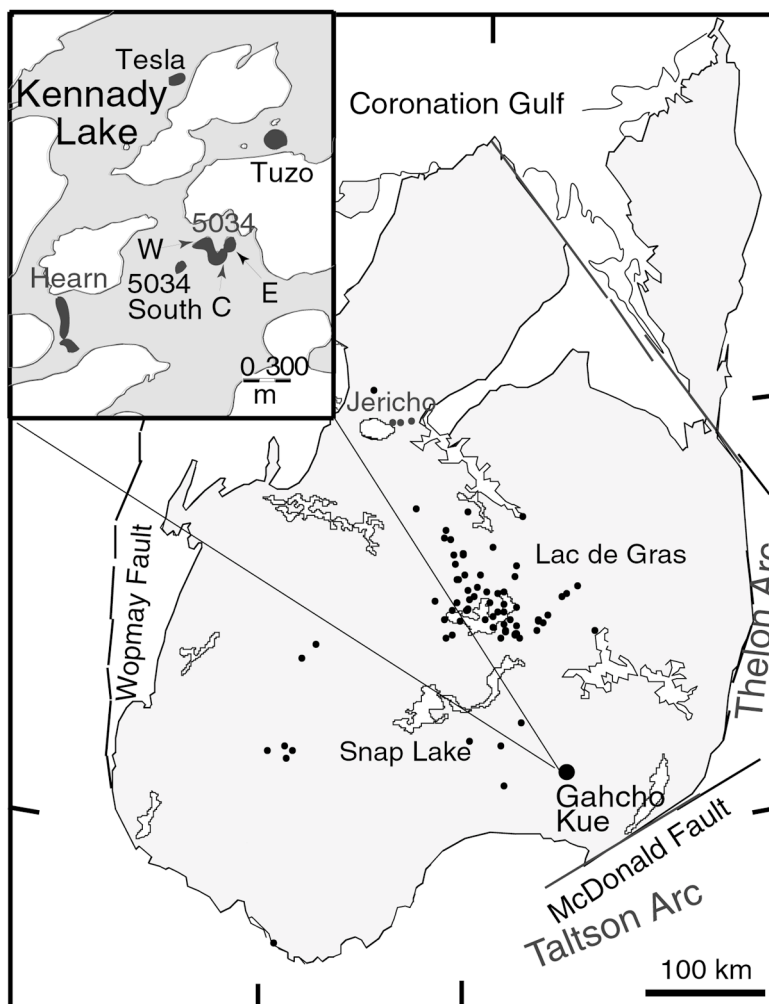


FIG. 1. Schematic map of the Slave craton showing location of the Gahcho Kue cluster and distribution of other Slave kimberlites. The inset illustrates distribution of kimberlites (black) within the cluster. All bodies intrude Archean granitic rocks and are submerged beneath lakes. The 5034 pipe consists of western (W), central (C), and eastern (E) lobes. The northern lobe intersected in the drill hole is not shown (B. Wyatt, pers. commun.).

Africa, but extremely different from those in many other Canadian kimberlites. The pipes formed by intrusive magmatic processes, and the depth of diatreme development in individual kimberlites at Gahcho Kue was variable. The pipes must have undergone significant erosion to strip away kimberlite down to the root zone (Hetman *et al.* 2003).

#### THE ARCHEAN BASEMENT

The kimberlites intrude unsubdivided Archean granitic rocks older than 2.4 Ga (Bethune *et al.* 1999) that

form the basement of the Slave craton. There is no evidence for any sedimentary cover at the time of kimberlite emplacement, as no sedimentary xenoliths were found in thorough petrographic studies of the Gahcho Kue kimberlite (this work, and Hetman *et al.* 2003).

Little is known about the Archean basement of the southeastern Slave Province. Geochemical data collected 70 km north of the Kennady Lake (at Wamsley Lake) show that the basement rocks are mostly granites with minor tonalite and granodiorite (Cairns *et al.* 2003). They are weakly peraluminous, have  $K_2O/Na_2O$  in the



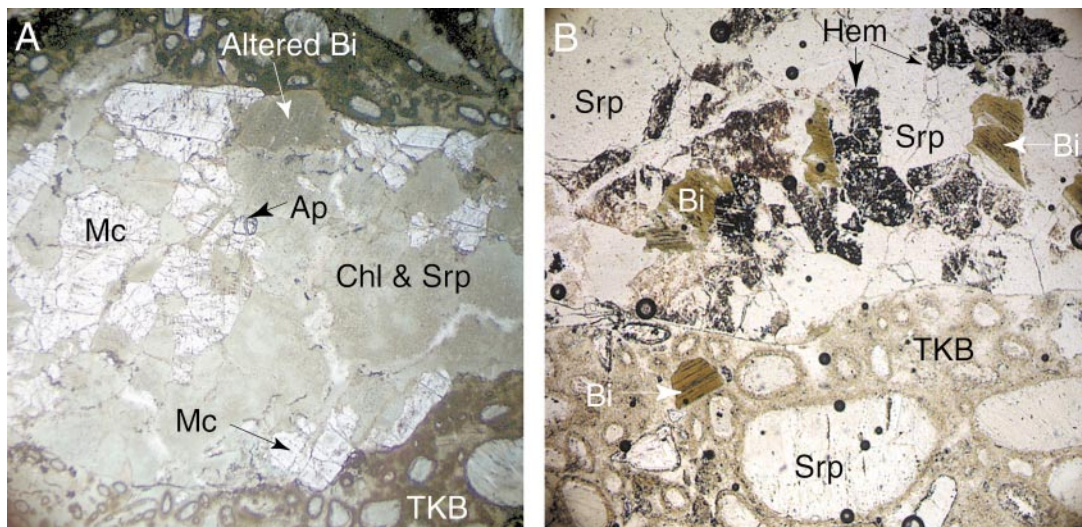


FIG. 3. Microphotographs of granitic xenoliths in the 5034 tuffisitic kimberlite breccia (TKB). All symbols here and on all figures are from Kretz (1983). A. An altered xenolith contain fresh microcline, identified by the tartan twinning, an aggregate of serpentine and chlorite replacing plagioclase and quartz, an aggregate of chlorite and epidote (?) replacing biotite, and fresh apatite. B. An altered xenolith comprising biotite, serpentine and grains replaced by serpentine intergrown with a black fine-grained mineral. The mineral is inferred to be hematite on the basis of its dark red color in the macrospecimen. The field of view is 2.6 mm in A and 5.2 mm in B.

or selectively altered. The alteration resulted in complete replacement of plagioclase and partial replacement of quartz by serpentine  $\pm$  chlorite  $\pm$  epidote and occasional pseudomorphs of chlorite  $\pm$  epidote after biotite (Fig. 3A). An alternative common pattern of alteration produces serpentine and fine-grained intergrowth of serpentine and hematite after felsic minerals (Fig. 3B). Xenocrysts of quartz, K-feldspar and biotite are occasionally found near the xenoliths and away from them. The whole-rock compositions of the granitic xenoliths (Table 1) indicate that they are strongly altered by addition of H<sub>2</sub>O (up to 8% wt.%) and MgO (15 wt.% MgO), serpentinized and cannot be representative of the southeastern Slave granitic basement.

The alteration of granite in the hypabyssal kimberlite is stronger and differs drastically from that in the tuffisitic kimberlite breccia. There is a marked reduction in size and abundance of the granite fragments that show significant reaction with the host kimberlite in all hypabyssal Gahcho Kue kimberlites (Hetman *et al.* 2003). Pervasive alteration and total "digestion" of the granites by the magmatic 5034 kimberlite are described below.

#### ANALYTICAL METHODS

Mineral modes of macrocrysts and microphenocrysts were estimated visually using the optical microscope. Proportions of groundmass phases were assessed on

SEM microphotographs *via* computer-assisted image analysis and averaged within each thin section.

The quantitative analysis of minerals (Tables 2–5 and Electronic Table 1) was performed with a fully automated CAMECA SX50 electron microprobe at the University of British Columbia. Acceleration voltage was 15 kV for phlogopite, spinel-group minerals and silicates, and 20 kV for perovskite. The beam current was set to 20 mA. On-peak counting times were 100 s for F, 80 s for rare-earth elements, 40 s for Nb and Th, and 20 s for all other elements. The micas were analyzed for alkalis in the first analytical session to minimize any possible underestimation. Note that the two Electronic Tables for this article are available from the Depository of Unpublished Data, CISTI, National Research Council, Ottawa, Ontario K1A 0S2, Canada.

Bulk-chemical analyses of the kimberlite were made at the McGill University Geochemical Laboratories (Montreal, Canada) and at the Chemex Laboratories (Vancouver, Canada). The samples were ground in a jaw crusher and then in a tungsten carbide ring mill with minimum grinding times. All major element, Cr and Ni contents were determined by X-ray fluorescence (XRF) spectrometry using a Philips PW2400 spectrometer on fused pellets. The concentration of ferrous iron was established by titration volumetrically. Concentrations of Rb and Zr were determined by X-ray fluorescence (XRF) spectrometry on pressed pellets, and those of other trace elements, by ICP–MS with sodium peroxide

fusion. Accuracy of XRF and ICP-MS analyses were checked against G2000 and SY4 standards, respectively. The precision of the major element and trace metal measurements is 5 and 10% relative.

Sm-Nd and Rb-Sr isotopic analyses were performed at the Radiogenic Isotope Facility at the University of Alberta. Small, carefully selected pieces of kimberlite were ground to remove visible xenolithic material, and then crushed to a fine powder. The powders were weighed, totally spiked with known amounts of mixed  $^{84}\text{Sr}$ - $^{87}\text{Rb}$  and  $^{149}\text{Sm}$ - $^{150}\text{Nd}$  tracers, and then Rb, Sr, Sm and Nd were separated by conventional ion-chromatography techniques (Holmden *et al.* 1996, Creaser *et al.* 1997). Determinations of Rb, Sr, Sm and Nd abundances and Sr and Nd isotopic compositions were made by isotope-dilution mass spectrometry using a Micro-

mass Sector 54 mass spectrometer. The long-term values for the SRM987 Sr and JNdi-1 Nd isotopic standards determined are  $0.710259 \pm 0.00002$  (1SD) and  $0.511210 \pm 0.000006$  (1SD), respectively. The Sr and Nd isotope data reported here are presented relative to values of 0.710245 for SRM987 and 0.512107 for JNdi-1. The latter is equivalent to a value of 0.511850 for the La Jolla Nd isotopic standard (Tanaka *et al.* 2000).

#### PETROGRAPHY

Within the hypabyssal kimberlite of the 5034 body, five characteristic rock-types can be distinguished: (1) aphanitic monticellite-serpentine kimberlite, (2) macrocrystal monticellite - phlogopite - serpentine kimberlite, (3) macrocrystal diopside- and monticellite-bearing phlogopite-serpentine kimberlite, (4) macrocrystal diopside- and melilite-bearing phlogopite-serpentine kimberlite, and (5) macrocrystal phlogopite-serpentine kimberlite.

Diopside-bearing kimberlite is described in three thin sections; two of them contain accessory monticellite, and one contains melilite. We do not know if diopside-bearing kimberlite constitutes two separate phases of hypabyssal kimberlite, or if the 5034 diopside-free kimberlite locally grades into the diopside-bearing varieties. The hypabyssal 5034 kimberlite is found in the main phase of the 5034 body, as well as in autoliths of the younger tuffisitic kimberlite breccia, which is in turn cut by macrocrystal phlogopite-serpentine kimberlite. The breccia contains ~30% pelletal lapilli made up of completely altered olivine, and felsic xenocrysts (3-5%) with thin selvages of magmatic kimberlite.

The macrocrystal phlogopite-serpentine kimberlite contains few country-rock xenoliths in contrast to the first four varieties of the hypabyssal kimberlite, which show similar patterns of alteration and assimilation of basement material. Xenoliths comprise ~1% of the kimberlite volume and include granite fragments and less abundant mantle nodules of peridotites, pyroxenites and eclogites (Kopylova & Caro, in press). The larger (more than 1 cm in size) granitic xenoliths are completely replaced by fine-grained serpentine, phlogopite and fibrous rosettes of pectolite growing inward. Xenoliths and xenocrysts may be surrounded by composite reaction coronae. The inner rim (~0.3 mm thick) is composed of long laths of diopside in radial aggregates. Such a diopside-dominant rim may be mantled by phlogopite (Fig. 4C) and it, in turn, is surrounded by a thicker, ~1 mm selvage of serpentinized host kimberlite (Fig. 4A). In this selvage, fresh olivine and monticellite are absent.

Visible granite xenoliths, however, represent only a minor part of the disaggregated felsic material. The rocks show evidence for assimilation of granitic microxenoliths, which are now observed as patches of distinctive mineralogy several mm<sup>2</sup> in area. These

TABLE 1. COMPOSITIONS OF GRANITES IN THE SOUTHEASTERN SLAVE PROVINCE AND ESTIMATES OF THE BULK COMPOSITION OF THE PRIMITIVE KIMBERLITIC MAGMA AND OF MODEL HYBRID ROCKS OF THE 5034 HYPABYSSAL KIMBERLITE

	SE Slave granite <sup>1</sup> <i>n</i> = 28	Granite xenolith BAK39148	Garnet peridotite <sup>2</sup> <i>n</i> = 8	Parental kimberlitic magma <sup>3</sup>	Model hybrid kimberlite <sup>4</sup>
SiO <sub>2</sub> wt.%	71.70	48.39	44.70	34.80	42.29
TiO <sub>2</sub>	0.32	0.31	0.11	1.55	0.86
Al <sub>2</sub> O <sub>3</sub>	14.69	14.70	1.64	4.28	4.29
Cr <sub>2</sub> O <sub>3</sub>		0.02	0.61	0.50	0.49
Fe <sub>2</sub> O <sub>3</sub> (total Fe)	1.59	4.54	7.14	9.00	7.53
MnO	0.03	0.05	0.12	0.22	0.16
MgO	0.80	15.39	43.90	27.90	31.37
CaO	1.84	1.00	1.56	7.11	4.41
Na <sub>2</sub> O	3.81	0.27	0.07	0.24	0.53
K <sub>2</sub> O	3.80	6.36	0.00	0.86	0.82
P <sub>2</sub> O <sub>5</sub>	0.14	0.16	0.05	0.78	0.43
LOI	0.54	8.14	0	11.36	5.85
Total	99.81	99.82	100.00	99.46	99.56
Ni, ppm	8	214	2141	838	1262.9
Ba	658	1868		2755	1470.8
Ce	76	71		361	191.5
Rb	153.8	91.9		87	59.8
Sr	269	322.5		793.2	431.4
Nb	11.7	7.7		308.3	158.4
Zr	176.3	137		144.2	91.1
Y	13	10.3		11.8	7.3
Ga	21.5	11.6		4.3	4.3
Pb		5.9		20.0	10.2
Th	20.9	6.7		36.6	20.7
U	4.8	<d.l.		11	6.1
Contam. Index				1.33	1.426
Mg#				84.8	

<sup>1</sup> Calculated as the average of 28 samples of granites in the Walmsley Lake area, 70 km north of the Kennady Lake (Cairns *et al.* 2003).

<sup>2</sup> Garnet peridotite composition is corrected for the effects of late alteration and normalized to 100% average bulk composition of the most common type of mantle xenolith in the 5034 kimberlite (Kopylova & Caro 2004).

<sup>3</sup> An estimate of the composition of the parental kimberlitic magma is calculated as the average of 5034 aphanitic kimberlites.

<sup>4</sup> Model kimberlite is calculated as 51% primitive kimberlitic magma + 10% granitic material + 39% garnet peridotite. The latter proportion is based on estimated 30% content of macrocrystal olivine in the 5034 hypabyssal kimberlite, and on the estimated 78% olivine in the garnet peridotite (Kopylova & Caro 2004). For model calculations, contents of trace elements (except Ni) are assumed to be negligible in the peridotite.

patches are characterized by: 1) complete absence or scarcity of groundmass opaque minerals and monticellite (Figs. 4B, D); 2) large crystals of calcite and strontian apatite apparently replacing grains in the plutonic xenoliths (Fig. 4D); 3) absence of greenish chlorite–serpentine and its local replacement by a colorless serpentine-group mineral; 4) abundant pectolite (Fig. 4B) or epidote (?) (the latter is seen as a high-relief fibrous Ca [± Fe, Al] silicate that forms tiny globular intergrowths); 5) occasional presence of barite in small (1–50 μm) anhedral grains associated with pectolite; 6) more abundant non-poikilitic phlogopite (Figs. 4B, D) that shows unusual zoning from a light orange to an orange-brown rim and is mantled by a thin (2 μm) layer of apatite; 7) occasional inclusions of long rectangular serpentinized laths interpreted as melilite pseudomorphs in poikilitic phlogopite, and 8) 1–2 mm haloes with complete serpentinization of olivine and monticellite around central patches of phlogopite.

The recognized varieties of the 5034 hypabyssal kimberlite are described below in the order of their inferred relative age of emplacement.

#### *Aphanitic monticellite – serpentine kimberlite*

This rock type is found in several distinct magmatic phases that precede or closely follow the emplacement of the macrocrystal monticellite – serpentine – phlogopite kimberlite. The aphanitic kimberlite comprises 1) angular autoliths included in the macrocrystal monticellite – serpentine – phlogopite kimberlite; 2) a thick (~3 cm) rim on the autoliths, and 3) ~10-cm-thick dikes cutting the macrocrystal monticellite – serpentine – phlogopite kimberlite.

In sample 48–K1, an angular autolith of the aphanitic kimberlite comprises the core of the large “snowball” globular segregation. Contacts between the core and the snowball rim are sharp and are accentuated by a difference in the degree of olivine alteration. Microphenocrysts of olivine are completely serpentinized in the core, but relatively fresh in the rim. Tangential orientation of olivine microphenocrysts controls the “snowball” texture of the rim. The rim contains several concentric layers 5–7 mm thick. The degree of olivine alteration and the abundance of phlogopite vary from one layer to the next. The contacts are sharp and accentuated by fine-grained veins of brown barite and a groundmass enriched in pectolite. Toward the sharp outer contact of the globular segregation, the olivine is progressively more serpentinized.

In sample 15–K1 (Fig. 4F), a 10-cm-thick dike cuts the macrocrystal monticellite – serpentine – phlogopite kimberlite. Contacts between them are sharp on one side and gradual on another. The sharp contact is defined by a sudden disappearance of olivine macrocrysts along a line of complex shape; however, the groundmass of the later aphanitic kimberlite does not show any signs of

thermal alteration or changes in grain size near the contact. On another contact, the dike kimberlite grades into the macrocrystal kimberlite over a few centimeters. Lenses of macrocrystal kimberlite are present in the dike and become more abundant toward the contact.

The groundmass of the aphanitic kimberlite (Fig. 5A) is composed mainly of euhedral olivine microphenocrysts (25%), a spinel-group mineral (<2%), monticellite (10–30%), phlogopite (0–5%); perovskite (<2%) and apatite (<2%) set in late-stage chlorite–serpentine (up to 25%) and pectolite (up to 15%), the latter being markedly more abundant than in macrocrystal samples. The aphanitic kimberlite differs drastically from the host macrocrystal kimberlite by its advanced degree of serpentinization of olivine and monticellite and the rarity of groundmass phlogopite.

#### *Macrocrystal monticellite – serpentine – phlogopite kimberlite*

This rock type is the dominant unit of the 5034 hypabyssal kimberlite. It contains 30% olivine and 70% groundmass. The groundmass consists of olivine microphenocrysts (7–15 vol.%), phlogopite plates (15–40 vol.%), euhedral monticellite (4–15 vol.%), a subhedral and euhedral spinel-group mineral (<2 vol.%), subhedral perovskite (<2 vol.%) and anhedral apatite (<2 vol.%) set in a base of late-stage chlorite–serpentine and chlorite (18–30 vol.%) (Fig. 5B). Accessory phases include anhedral calcite, pectolite, epidote (?), barite and apatite.

Olivine macrocrysts (more than 0.5 mm in size) are rounded, and partly or completely replaced by carbonate and serpentine, and mantled by large plates of groundmass phlogopite. The subhedral to euhedral microphenocrysts (0.1–0.5 mm) may be rimmed by individual grains of a spinel mineral, perovskite or monticellite. Phlogopite is typically present in large (0.1–0.5 mm) poikilitic groundmass crystals that commonly host numerous inclusions of monticellite, chromian spinel and olivine microphenocrysts. Included silicates may be replaced by serpentine. Phlogopite is strikingly zoned in some samples, and seems homogeneous in others. The most common observed zoning is from a pleochroic orange-yellow core to a colorless rim (Fig. 4D). This transition in color may be gradual or sharp, and is seen in poikilitic phlogopite and in rarer, smaller, non-poikilitic grains. The spinel-group mineral occurs as minute (1–50 μm), rounded to euhedral grains included in phlogopite, monticellite, chlorite–serpentine, or pectolite. Atoll-textured spinel, a hallmark of Group-I kimberlites, is extremely rare. Perovskite commonly occurs as small (10–20 μm) euhedral homogeneous groundmass crystals. Grains are usually set in late-stage chlorite–serpentine or poikilitic phlogopite, and can be found crystallized around olivine microcrysts or overgrown upon an earlier generation of the spinel-

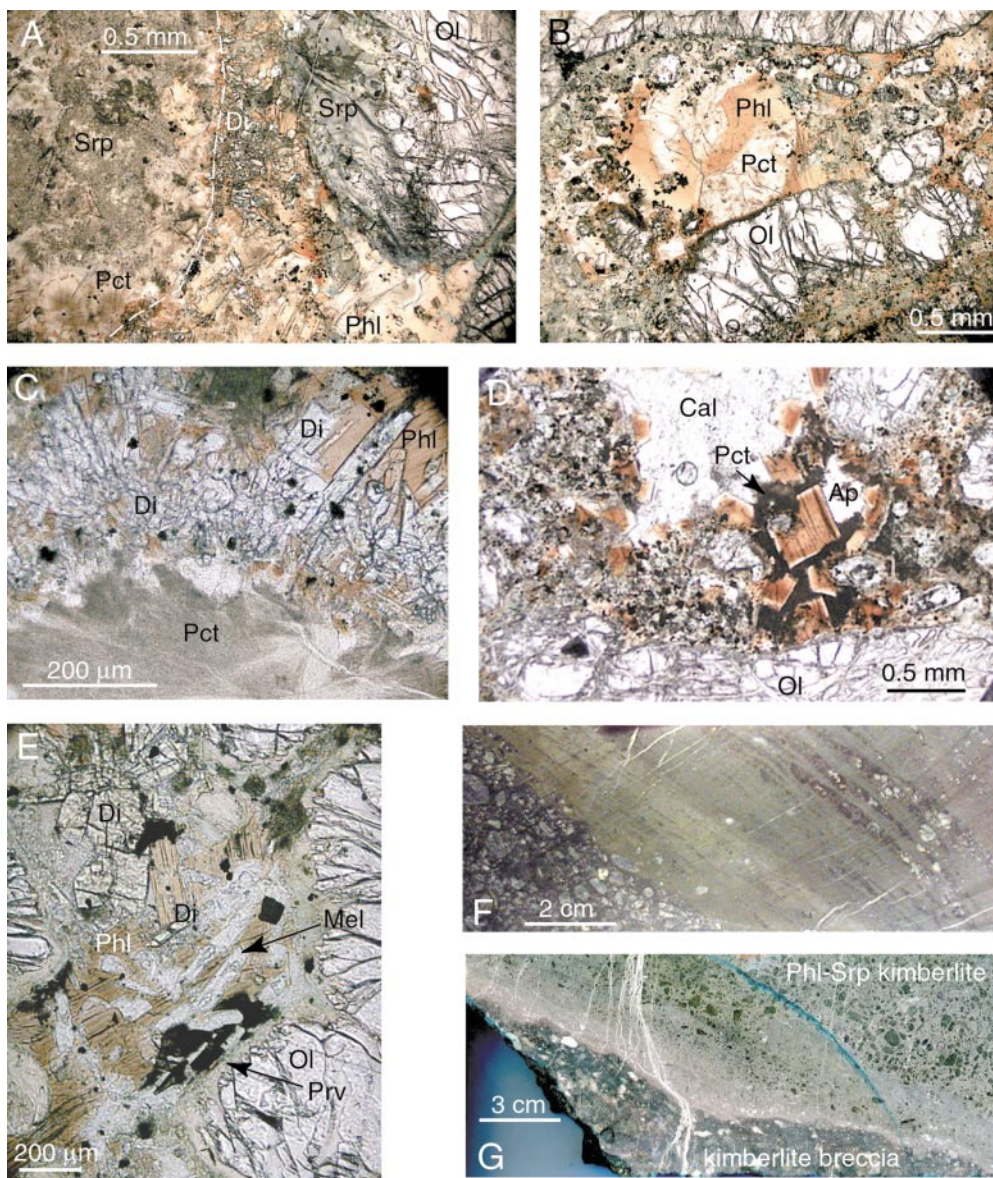


FIG. 4. Photographs illustrating textures of the 5034 kimberlite and contact relationships between different rock-types. A. A granitic xenolith (dashed outline) replaced by serpentine and spherulitic aggregates of pectolite is surrounded by diopside and serpentine. Note uneven serpentinization of the adjacent olivine macrocryst only in contact with the corona diopside. B. Distinct groundmass of the macrocrystal kimberlite replaces an assimilated granitic xenolith. The area comprises pectolite and non-poikilitic phlogopite and is devoid of opaque minerals. Note the characteristic zoning of phlogopite, from an orange core to a dark reddish rim typical of diopside-bearing kimberlite. C. A zoned corona on a xenolith replaced by fibroradial pectolite. The inner layer of diopside is mantled by phlogopite. D. Distinct groundmass of the macrocrystal kimberlite replaces an assimilated granitic xenolith. The area comprises calcite, an aggregate of fibrous pectolite and zoned phlogopite, and is devoid of opaque minerals. Colorless phlogopite mantles grow on orange phlogopite cores; a larger crystal also displays a gradual change to a lighter yellow core. E. Laths of serpentinized melilite in phlogopite and perovskite coexist with fresh diopside in the groundmass of diopside- and melilite-bearing kimberlite. F. A dike of aphanitic kimberlite cuts macrocrystal kimberlite on one side and grades into macrocrystal kimberlite on another side. The macrocrystal kimberlite appears in lenses that gradually become more abundant and coalesce. G. The "chilled margin" contact between younger phlogopite – serpentine kimberlite and tuffitic kimberlite breccia.

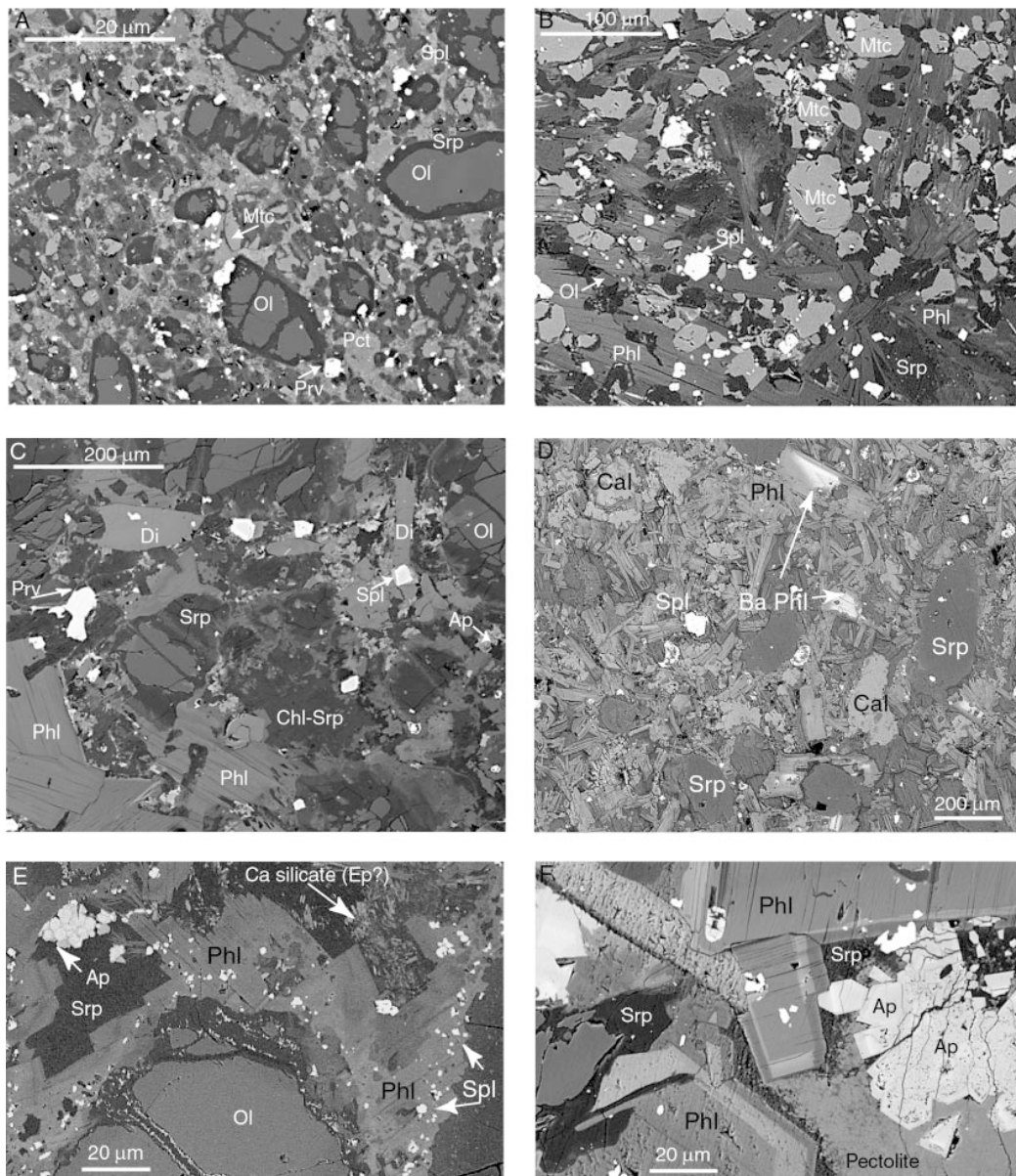


FIG. 5. SEM microphotographs illustrating textures of the 5034 kimberlite. A. Aphanitic monticellite–serpentine kimberlite. Large subhedral and euhedral olivine microphenocrysts are set in a finer-grained groundmass. The groundmass is typically composed of a late anhedral pectolite, serpentinized monticellite, subhedral perovskite and a spinel-group mineral. Note that phlogopite and a late-stage chlorite–serpentine are absent and pectolite is ubiquitous. B. The groundmass of macrocrystalline phlogopite–serpentine kimberlite. Monticellite, spinel and perovskite are set in large tabular crystals of phlogopite. Serpentine replaces monticellite and olivine. C. Diopside-bearing macrocrystalline kimberlite. Phlogopite microphenocrysts, serpentinized olivine, euhedral diopside and spinel-group minerals, subhedral perovskite and apatite are set in a late-stage chlorite–serpentine. The largest spinel-group minerals display a slightly darker core of chromite zoned to a brighter rim of magnetite. Fresh monticellite is markedly absent from the rock. D. Groundmass of phlogopite – serpentine kimberlite. Note abundant calcite and cores of light barian phlogopite in larger phlogopite crystals. E. Patchy zoning of phlogopite in sample 39–270. Darker areas of Fe-enriched phlogopite occur in contact with fine laths of Ca silicate and apatite. F. Two generations of phlogopite rims in sample 8–K4. The uneven development of the latest Na-rich phlogopite is controlled by its neighboring minerals. The dark Fe- and Na-rich outer rim grows in contact with serpentine, but is absent next to pectolite.

group mineral. Apatite may occur as small (<100  $\mu\text{m}$ ) anhedral to euhedral groundmass crystals or granular aggregates (Fig. 5E). The late-stage phase (18–30%) can either be poikilitic phlogopite or chlorite–serpentine, both of which form segregated patches with various amounts of pectolite.

*Macrocrystal diopside- and monticellite-bearing phlogopite – serpentine kimberlite*

This rock type (Fig. 5C) is distinguished from the dominant 5034 hypabyssal kimberlite by the presence of diopside, relatively more abundant apatite and pectolite, and a complete serpentinization of monticellite. Large rounded olivine macrocrysts (30%) are set in a uniformly textured groundmass of olivine microphenocrysts (15%), phlogopite (30%), chlorite–serpentine (7%), altered monticellite (at least 4%), diopside (1%), spinel-group mineral and perovskite (2%), apatite (2%) and pectolite (7%). The mode of the replaced monticellite is hard to determine since it is masked by chlorite–serpentine of the groundmass and is conspicuous only if included in phlogopite oikocrysts. Phlogopite occurs as large (100–500  $\mu\text{m}$ ) tabular oikocrysts and as small (10–100  $\mu\text{m}$ ) euhedral non-poikilitic crystals. Phlogopite crystals are commonly mantled by chlorite–serpentine and enclose the fresh spinel-group mineral and diopside, and altered olivine and monticellite. The phlogopite is strongly zoned, with a reddish rim and pale orange core (Fig. 4B). This pattern is clearly distinct from the one observed in the dominant diopside-free hypabyssal kimberlite. The most pronounced zoning is displayed in phlogopite grains that grow around partly “digested” granitic xenoliths (Fig. 4D). The contact between the outer rim (10–20 mm) of reddish phlogopite and the orange core is sharp; furthermore, two distinct rims of overgrowth are occasionally seen on phlogopite. The presence and the thickness of the rims are controlled by minerals in contact with phlogopite (Fig. 5F). Diopside is unevenly distributed throughout the sample and forms microphenocrysts (up to 0.6 mm) and fresh small (10–50  $\mu\text{m}$ ) greenish prismatic and lath-like crystals in the groundmass.

*Macrocrystal diopside- and melilite-bearing phlogopite – serpentine kimberlite*

This rock type is described in only one sample, 61–K2, which represents a large (4 cm) autolith in kimberlite breccia. This variety of hypabyssal kimberlite stands out owing to the high modal abundance of euhedral diopside and chlorite–serpentine, relatively scarce pectolite, and the presence of serpentinized melilite (?). The latter is identified by its long rectangular shapes of laths that have square terminations (Fig. 4E), unlike those of calcite. The kimberlite consists of olivine macrocrysts (15%) and a groundmass of olivine microphenocrysts (20%), chlorite–serpentine (35%),

phlogopite (20%), diopside (4–8%), a spinel-group mineral and perovskite (2%), altered melilite (2%?), and traces of monticellite, apatite and pectolite. Phlogopite forms large homogeneous oikocrysts and rarer zoned grains without inclusions, and overgrows diopside crystals. The zoning is observed as a brown rim on an orange core. The oikocrysts poikilitically enclose diopside, serpentinized melilite and monticellite, olivine, the spinel, and apatite (listed in the order of their abundance in phlogopite crystals). Melilite is replaced by a colorless serpentine-group mineral with a mottled low birefringence. Melilite and monticellite are visible only if included in phlogopite or an opaque mineral, and comprise 10% and 1% of its volume, respectively. Diopside occurs in euhedral microphenocrysts and in smaller groundmass crystals set in late-stage chlorite–serpentine (Fig. 4E). Chromite, apatite and perovskite are commonly included in diopside microphenocrysts.

*Macrocrystal phlogopite – serpentine kimberlite*

This rock type was emplaced last and cuts the tuffisitic breccia along a wavy irregular contact. The kimberlite grades from aphanitic (2 cm from the contact) to macrocrystal (away from the contact) (Fig. 4G). The aphanitic kimberlite gradually changes its color from brown-grey (5 mm from the contact) to greenish grey. Consistent variations in color and grain size in the kimberlite are compatible with its chilled margin origin. Rare macrocrysts in the aphanitic kimberlite are oriented parallel to the contact. The groundmasses of the aphanitic and macrocrystal kimberlites are similar, the only difference being the presence of 25% totally serpentinized olivine macrocrysts in the latter. The groundmass is composed of 25% serpentinized olivine microphenocrysts, 25% phlogopite, 20% chlorite–serpentine and chlorite, 4–8% calcite, ~5% serpentinized monticellite and minor spinel mineral and apatite (Fig. 5D). This variety of the kimberlite is characterized by colorless phlogopite that crystallizes in rosette aggregates of non-poikilitic grains, and relatively abundant calcite.

#### MINERAL COMPOSITIONS

Phlogopite varies greatly in composition from one rock type to another, from sample to sample within one rock type, and even over distances as small as 20  $\mu\text{m}$ . To illustrate this compositional variability and to identify the major factors that control it, we describe the mineralogy and zoning patterns of phlogopite separately in all sample groups (see Appendix). Representative compositions of phlogopite are given in Table 2, whereas complete datasets of analytical results have been sent to the Depository of Unpublished Data, CISTI, National Research Council, Ottawa, Ontario K1A 0S2 and can be downloaded from <http://www.eos.ubc.ca/public/people/faculty/kopylova/data.html>.

Olivine microphenocrysts and macrocrysts consist of forsterite (Fo<sub>89</sub>–Fo<sub>92</sub>) containing 0.2–0.4 wt.% NiO (Table 3). The entire range of olivine compositions can be found in one sample in the microphenocryst population. There is no systematic difference in composition between macrocrysts and phenocrysts, but the former display a rare irregular patchy zoning.

The spinel-group mineral was analyzed in monticellite-rich varieties of the kimberlite in areas free of assimilated felsic material. Representative compositions of the mineral are given in Table 3; complete datasets of analytical results can be found in the Depository of Unpublished Data, CISTI, and at <http://www.eos.ubc.ca/public/people/faculty/kopylova/data.html>. Grains larger than 20  $\mu\text{m}$  have a discrete magnesiochromite core and a 10  $\mu\text{m}$  mantle of titanian magnetite. Smaller grains (<10  $\mu\text{m}$ ) are typically homogeneous and similar in composition to the late titanian magnetite. All spinel-group mineral compositions form a broad single combined trend in the reduced spinel prism, with chromite and titanian magnetite in diopside-bearing kimberlites displaying higher molar fractions of Fe<sup>2+</sup> and Ti<sup>4+</sup> (Fig. 6). Early magnesiochromite is characterized by low Fe<sup>2+</sup>/(Fe<sup>2+</sup> + Mg) and Ti/(Ti + Al + Cr) values. Compositions evolve toward higher Cr/(Cr + Al) and Fe<sup>2+</sup>/(Fe<sup>2+</sup> + Mg) values. Intermediate compositions display high and constant Cr/(Cr + Al) values, and show a trend of increasing Fe<sup>2+</sup>/(Fe<sup>2+</sup> + Mg) and Ti/(Ti + Cr + Al). The most evolved compositions (magnetite) are characterized by high Ti/(Ti + Al + Cr) and Fe<sup>2+</sup>/(Fe<sup>2+</sup>

+ Mg) values and evolve along a trend of decreasing Ti/(Ti + Al + Cr). The Mn content is low (0.1 to 1.2 wt.% MnO) and increases from core to rim. Zoning trends within individual samples conform to the overall trend. However, the spinel-group mineral in the individual samples shows a wide range of core compositions, with  $X_{\text{Cr}} = \text{Cr}/(\text{Cr} + \text{Al})$  between 0.66 and 0.90. An equally wide range of compositions, with  $X_{\text{Ti}} = \text{Ti}/(\text{Ti} + \text{Cr} + \text{Al})$  in the range 0.2–0.85, is displayed by the rim, and compositional gaps between core and rim vary greatly. The most pronounced contrast between core and rim spinel is noted in sample 61–K2, where late magnetite is unusually Al- and Ti-rich (Table 3).

Pectolite shows moderate variations in Al (0–0.3 wt.% Al<sub>2</sub>O<sub>3</sub>), Fe (0.3–1 wt.% FeO) and Mg (0.2–1.3 wt.% MgO), and is almost perfectly stoichiometric (Table 3).

Diopside found in the groundmass and in reaction coronas is similar in composition. It contains moderate Cr (0.2–0.5 wt.% Cr<sub>2</sub>O<sub>3</sub>), Ti (0.1–0.7 wt.% TiO<sub>2</sub>) and Fe (1–3.5 wt.% FeO, total). Despite major differences in petrography among the samples, their diopside is almost identical (Table 4) and closely resembles Al- and Fe-poor diopside found in Group-I kimberlites (Mitchell 1995). In contrast, diopside in sample 61–K2 is significantly enriched in Fe, Ca and Ti, and lower in Cr. The Ti-rich character of this diopside follows the compositional pattern found in the same sample for the spinel-group mineral and phlogopite, and may be a result of the overall higher bulk Ti in the 61–K2 magma. Diop-

TABLE 2. REPRESENTATIVE COMPOSITIONS OF PHLOGOPITE IN THE 5034 HYPABYSSAL KIMBERLITE, N.W.T.

Sample	Comment	SiO <sub>2</sub>	TiO <sub>2</sub>	Al <sub>2</sub> O <sub>3</sub>	Cr <sub>2</sub> O <sub>3</sub>	FeO(t)	MnO	MgO	CaO	Na <sub>2</sub> O	K <sub>2</sub> O	BaO	Cl	F	Total
21-K4	Core	41.45	3.48	2.58	0.01	9.44	0.19	20.96	0.08	0.80	14.79	0.85	0.02	1.56	96.21
21-K4	Core, Ba-poor patches	41.16	0.25	9.07	0.00	6.54	0.08	26.27	0.04	0.04	10.41	0.52	0.00	0.10	94.49
21-K4	Rim	38.57	2.59	6.25	0.00	10.29	0.22	23.66	0.04	0.17	9.37	2.98	0.00	0.86	95.00
21-K4	Rim, outer 10 mm	37.54	0.63	9.77	0.00	23.87	0.48	12.49	0.10	0.07	9.73	0.05	0.00	0.00	94.72
39-270	Rim, homogeneous	41.06	1.43	8.06	0.00	8.09	0.05	24.93	0.02	1.14	9.74	0.12	0.00	0.70	95.36
39-270	Rim, one grain	41.67	0.05	11.47	0.01	6.59	0.27	24.50	0.01	0.09	10.63	0.01	0.02	0.00	95.33
39-270	Core, one grain	41.07	1.24	7.99	0.00	8.60	0.13	24.69	0.09	1.12	10.34	0.14	0.04	0.52	95.96
39-270	Core next to pect.	41.25	0.03	2.10	0.01	12.07	0.04	28.00	0.20	0.00	9.57	0.05	0.30	0.00	93.64
39-270	Rim next to Sr Ap.	42.63	0.26	9.27	0.04	5.62	0.07	26.54	0.02	0.43	10.76	0.06	0.05	0.28	96.03
39-270	Core pseudomorph after granite	41.08	1.84	7.92	0.00	8.96	0.08	24.14	0.15	1.17	10.06	0.24	0.01	1.24	96.88
8-K4	Core, one grain	41.27	1.75	10.57	0.08	4.94	0.05	25.11	0.05	0.18	10.27	1.14	0.04	2.27	97.72
8-K4	Rim, one grain	41.44	0.37	0.04	0.07	15.17	0.09	26.10	0.03	0.09	10.47	0.18	0.00	0.00	94.04
8-K4	Rim, outer 5 mm	49.74	0.35	0.52	0.03	6.27	0.14	26.60	0.22	0.50	9.41	0.43	0.00	0.00	94.21
61-K2	Core, Phl mantle on diopside	39.26	0.84	7.52	0.02	9.29	0.15	26.95	0.12	0.09	6.80	0.52	0.01	0.18	91.75
61-K2	Core	37.40	4.60	12.73	0.13	6.83	0.03	21.15	0.00	0.19	9.50	2.31	0.00	1.34	96.22
11-K5D	Core, one grain	31.41	1.36	17.13	0.00	4.68	0.05	22.29	0.02	0.11	7.02	9.45	0.00	0.17	93.69
11-K5D	Rim, one grain	37.99	0.82	11.14	0.01	7.47	0.05	26.29	0.08	0.09	8.09	0.86	0.02	0.31	93.21

Symbols: Sr Ap: strontian apatite, Phl: phlogopite, pect: pectolite.

TABLE 3. REPRESENTATIVE COMPOSITIONS OF OLIVINE, SPINEL AND PECTOLITE IN THE 5034 HYPABYSSAL KIMBERLITE, N.W.T.

Sample No	Olivine				Spinel						Pectolite		
	micro-pheno. 21-K2	macro-cryst 8-K4	core 61-K2	rim 61-K2	core 21-K2	rim 21-K2	rim 21-K2	core 39-270	rim 39-270	rim 39-270	core 8-K4	rim 8-K4	rim 8-K4
SiO <sub>2</sub> wt. %	40.50	40.59	0.18	0.05	0.17	0.10	0.39	0.11	0.30	0.06	0.08	0.71	52.96
TiO <sub>2</sub>	0.02	0.01	2.08	9.37	2.50	5.75	2.85	2.27	1.46	6.35	1.87	5.58	0.13
Al <sub>2</sub> O <sub>3</sub>	0.01	0.01	12.36	0.29	8.91	0.44	0.23	8.24	0.15	0.44	6.55	0.13	0.02
Cr <sub>2</sub> O <sub>3</sub>	0.03	0.03	49.58	1.32	51.70	15.23	1.08	52.92	0.90	9.47	53.78	1.15	0.00
Fe <sub>2</sub> O <sub>3</sub>	-	-	6.66	51.85	6.32	44.77	64.77	6.26	67.67	49.05	6.76	56.29	
FeO	9.63	10.53	13.94	30.02	18.06	24.86	20.43	16.80	21.72	27.14	20.77	31.29	1.03
MnO	0.16	0.15	0.10	0.46	0.36	0.67	0.79	0.35	0.82	1.09	0.76	1.06	0.20
MgO	48.22	47.46	13.96	5.56	11.12	6.86	7.75	11.52	6.25	5.39	8.42	2.86	0.99
CaO	0.08	0.04	0.06	0.29	0.11	0.09	0.23	0.10	0.14	0.27	0.00	0.14	28.77
NiO	0.35	0.31	0.32	0.37	0.08	0.36	0.55	0.17	0.47	0.23	0.09	0.08	
Na <sub>2</sub> O													9.57
H <sub>2</sub> O													2.62
Total	99.00	99.14	99.25	99.58	99.32	99.14	99.07	98.74	99.88	99.49	99.08	99.27	96.29
Si <i>apfu</i>	1.003	1.007	0.010	0.002	0.006	0.000	0.010	0.000	0.010	0.020	0.003	0.027	3.026
Ti	0.000	0.000	0.050	0.258	0.062	0.160	0.080	0.060	0.040	0.180	0.048	0.158	0.006
Al	0.000	0.000	0.470	0.013	0.349	0.020	0.010	0.320	0.060	0.020	0.265	0.006	0.001
Cr	0.001	0.001	1.260	0.0038	1.357	0.440	0.030	1.400	0.030	0.270	1.459	0.034	0.000
Fe <sup>3+</sup>	0.199	0.219	0.160	1.429	0.158	1.220	1.780	0.160	1.870	1.1350	0.175	1.591	
Fe <sup>2+</sup>	-	-	0.380	0.920	0.501	0.760	0.620	0.470	0.670	0.830	0.596	0.983	0.049
Mn	0.004	0.003	0.000	0.014	0.010	0.020	0.020	0.010	0.030	0.030	0.022	0.034	0.010
Mg	1.780	1.755	0.670	0.304	0.550	0.370	0.420	0.570	0.340	0.290	0.431	0.16	0.084
Ca	0.002	0.001	0.000	0.011	0.004	0.000	0.010	0.000	0.050	0.010	0.000	0.006	1.761
Ni	0.007	0.006	0.010	0.011	0.002	0.010	0.020	0.010	0.010	0.070	0.002	0.002	
Na													1.060
H													1.000
Cation sum	2.996	2.992	3.000	3.000	3.000	3.000	3.000	3.000	3.000	3.000	3.000	3.000	5.998

The proportion of ferric iron is recalculated assuming perfect stoichiometry using the FORMULA software; the amount of H<sub>2</sub>O is calculated based on one H<sup>+</sup>.

side in all samples shows moderate between-grain chemical variations (up to 1.5 wt.% TiO<sub>2</sub>, Al<sub>2</sub>O<sub>3</sub> and FeO) and, occasionally, an irregularly shaped, chemically distinct core.

Monticellite is homogeneous and has the general formula Mg<sub>0.9</sub>Ca<sub>0.9</sub>Fe<sub>0.2</sub>SiO<sub>4</sub> (Table 4).

The serpentine-group mineral (lizardite?) varies strongly in Fe (2–7 wt.% FeO), Ca (0.1–1.5 wt.% CaO) and Al (0–1.5 wt.% Al<sub>2</sub>O<sub>3</sub>) contents. Serpentine replacing olivine is devoid of these elements, whereas ground-mass chlorite–serpentine is higher in Al, Fe and Ca. There is no compositional continuity between ground-mass chlorite–serpentine and the more Al- and Fe-rich chlorite that replaces phlogopite (Table 4).

Perovskite (Table 5) is typically Fe-, Nb- and Na-poor and selectively enriched in Ce compared to La (2–

3 wt.% Ce<sub>2</sub>O<sub>3</sub> versus 1 wt.% La<sub>2</sub>O<sub>3</sub>) and all other REE [5–6 wt.% (REE)<sub>2</sub>O<sub>3</sub>]. Perovskite shows no between-grain and within-grain compositional variance in three samples studied, but in sample 48–K1, its composition depends on that of the neighboring mineral. If perovskite is found next to pectolite, it has increased contents of Nb, Ti, Sr, and Na, and decreased contents of Fe, Th, Al, Ce and Ca.

Apatite is commonly homogeneous, but the larger crystals are zoned, with a distinct Sr-enriched core and Na-enriched rim. In areas of assimilated felsic material, apatite is more likely to have a Sr-rich core.

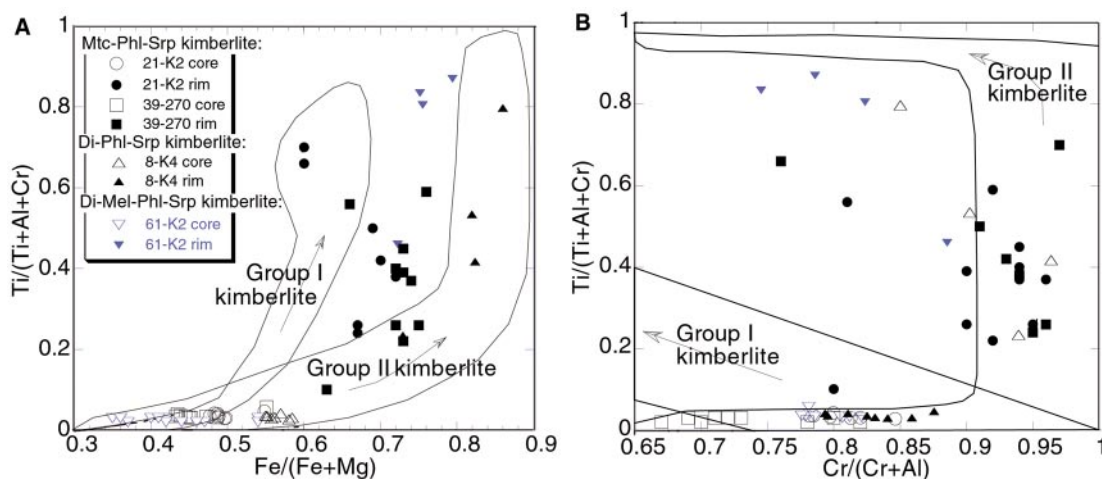


FIG. 6. Plots of the front (a) and bottom (b) faces of the reduced spinel prism [ $Ti/(Ti + Al + Cr)$  versus  $Fe^{2+}/(Fe^{2+} + Mg)$  and  $Ti/(Ti + Al + Cr)$  versus  $Cr/(Cr + Al)$ ] illustrating the compositional trend of spinel-group minerals from the Gahcho Kue kimberlite. Open fields indicate the evolutionary trends of spinel-group minerals in Group-I kimberlites (Magmatic Trend 1) and Group II kimberlites (Magmatic Trend 2) (Mitchell 1995).

#### BULK AND ISOTOPIC COMPOSITION OF THE 5034 KIMBERLITE

The major- and minor-element compositions of the rock types of the 5034 kimberlite (Table 6) characterize it as a Group-IA kimberlite, as defined by  $SiO_2$ , Pb,  $TiO_2$ , and  $K_2O$  contents (Smith *et al.* 1985). The Pb contents are low (4–14 ppm in all samples except the aphanitic variety) characteristic of Group-I kimberlites, but  $SiO_2$  contents are relatively high (37–42 wt%  $SiO_2$ ). A trend of correlated  $K_2O$  and  $TiO_2$ , diagnostic of mica-bearing kimberlites, extends very little into the Group-II kimberlite field, which expands to 7 wt.%  $K_2O$  (Fig. 7A). The Contamination Index (CI), useful for detecting contamination of kimberlites by silicate xenoliths and xenocrysts, is below 1.5, which is in the range of uncontaminated kimberlites (Mitchell 1986). The tuffitic kimberlite breccia has a higher CI (1.3–1.4) than the hypabyssal kimberlite (1.1–1.3). High Mg-numbers (85–92) of the rocks indicate that they are not the product of a primary mantle-derived magma, but are contaminated by abundant Mg-rich olivine. Almost all samples of 5034 kimberlite has a  $Fe_2O_3/FeO$  ratio equal to 0.5–1.25, which is very low for Group-I kimberlites ( $Fe_2O_3/FeO$  in the range 1–2) and is more typical of micaceous Group-II kimberlites ( $Fe_2O_3/FeO$  in the range 0.4–1.7). However, other Group-I kimberlites in the Slave craton have similarly low Fe ratios ( $Fe_2O_3/FeO$  in the range 0–1 at Jericho and 0.5–0.8 at Ranch Lake).

The 5034 kimberlite shows a pattern of strong overall enrichment in incompatible elements with respect to

TABLE 4. REPRESENTATIVE COMPOSITIONS OF DIOPSIDE, MONTICELLITE, SERPENTINE AND CHLORITE IN THE 5034 HYPABYSSAL KIMBERLITE, N.W.T.

Sample No.	Diopside				Monticellite	Serpentine		Chlorite after Phl
	20-K3	61-K2	8-K4	8-K4	21-K4	after Ol	ground-mass	15-K5D
$SiO_2$ wt.%	54.16	52.48	53.66	54.09	36.11	38.65	38.43	31.14
$TiO_2$	0.13	1.77	0.33	0.20	0.11	0.02	0.02	0.34
$Al_2O_3$	0.06	1.05	0.14	0.12	0.03	0.02	1.36	9.12
$Cr_2O_3$	0.14	0.02	0.24	<d.l.	0.19	<d.l.	0.06	<d.l.
FeO	1.45	5.49	2.48	1.90	9.04	2.04	4.10	14.44
MnO	0.04	0.08	0.08	0.08	0.34	0.05	0.18	0.04
MgO	17.80	15.09	17.04	17.54	21.06	41.16	34.61	28.30
CaO	24.30	23.25	24.56	24.43	32.26	0.07	1.33	0.18
NiO	0.12	<d.l.	<d.l.	0.09	0.08	0.33	0.47	-
$Na_2O$	-	0.85	-	-	-	-	-	0.05
$K_2O$	-	0.04	-	-	-	-	-	0.98
Total	98.21	100.16	98.29		99.22	82.33	80.55	84.60

<d.l.: below detection limit; -: not analyzed.

the primitive mantle. This pattern, with a pronounced K trough, is typical of Group-I and Group-II kimberlites (Fig. 8). On the Zr–Nb plot (Fig. 7B), all samples of the 5034 kimberlite, except the aphanitic type, fall into the field reported for Group-I kimberlites. The aphanitic 5034 kimberlite has a very low Zr/Nb ratio for a Group-I kimberlite ( $Zr/Nb = 0.5$ ) similar to that in aphanitic samples of the Jericho kimberlite (Kopylova *et al.* 1998). These ratios resemble low values of Zr/Nb (0.25;

Fig. 7B) in a complex mica-rich Aries kimberlite (Australia) intermediate between Group-I and -II kimberlites (Edwards *et al.* 1992).

Geochemical data confirm divisions identified petrographically and mineralogically within the 5034 pipe. Four rock types within the kimberlite are distinct geochemically: hypabyssal macrocrystal monticellite – phlogopite – serpentine kimberlite (with or without diopside), hypabyssal phlogopite–serpentine kimberlite, aphanitic kimberlite, and tuffisitic kimberlite breccia. The aphanitic kimberlite stands out by its low SiO<sub>2</sub>, Ni, and Mg-number, and high levels of TiO<sub>2</sub>, Al<sub>2</sub>O<sub>3</sub>, Cr<sub>2</sub>O<sub>3</sub>, MnO, P<sub>2</sub>O<sub>5</sub>, Ba, Sr, Nb, Zr, Ce, Pb, Th, and U. Its geochemical traits are easily explained by less dilution from olivine xenocrysts compared to the macrocrystal kimberlites. The kimberlite breccia has lower levels of P<sub>2</sub>O<sub>5</sub>, CO<sub>2</sub>, CaO and Cr<sub>2</sub>O<sub>3</sub>, and higher SiO<sub>2</sub>. The hypabyssal phlogopite–serpentine kimberlite differs by higher CO<sub>2</sub>, lower Al<sub>2</sub>O<sub>3</sub> and a higher Fe<sub>2</sub>O<sub>3</sub>/FeO ratio equal to 2 (Table 6). The presence or absence of diopside in the hypabyssal kimberlite does not correlate with its bulk composition.

TABLE 5. REPRESENTATIVE COMPOSITIONS OF PEROVSKITE, IN THE 5034 HYPABYSSAL KIMBERLITE, N.W.T.

Sample No Average of	61-K2 22	15-K1 12	39-270 5	48-K1 5*	48-K1 5
Nb <sub>2</sub> O <sub>5</sub>	1.12	0.98	0.97	1.64	0.95
TiO <sub>2</sub>	51.52	51.96	51.73	52.34	51.43
ThO <sub>2</sub>	0.40	0.48	0.42	0.12	0.50
Al <sub>2</sub> O <sub>3</sub>	0.51	0.45	0.46	0.19	0.46
La <sub>2</sub> O <sub>3</sub>	1.22	1.14	1.14	1.32	1.18
Ce <sub>2</sub> O <sub>3</sub>	2.61	2.73	2.60	2.14	2.74
Pr <sub>2</sub> O <sub>3</sub>	0.28	0.30	0.29	0.21	0.29
Nd <sub>2</sub> O <sub>3</sub>	0.90	0.87	0.88	0.63	0.93
Sm <sub>2</sub> O <sub>3</sub>	0.08	0.10	0.08	0.09	0.08
Gd <sub>2</sub> O <sub>3</sub>	0.09	0.04	0.14	0.04	0.05
FeO	2.88	2.32	2.50	1.82	2.47
MnO	0.02	0.01	0.01	0.01	0.01
MgO	0.25	0.11	0.09	0.11	0.37
CaO	35.65	35.58	35.90	34.96	35.64
SrO	0.36	0.29	0.25	1.60	0.27
Na <sub>2</sub> O	0.33	0.35	0.33	0.68	0.36
Total	98.23	97.71	97.80	97.89	97.70
Nb <i>apfu</i>	0.012	0.011	0.011	0.018	0.010
Ti	0.936	0.890	0.942	0.951	0.938
Th	0.002	0.002	0.002	0.001	0.003
Al	0.015	0.036	0.013	0.005	0.013
La	0.011	0.009	0.010	0.012	0.011
Ce	0.023	0.021	0.023	0.019	0.024
Pr	0.003	0.002	0.003	0.002	0.003
Nd	0.008	0.007	0.008	0.005	0.008
Sm	0.001	0.001	0.001	0.001	0.001
Gd	0.001	0.000	0.001	0.000	0.000
Fe (total)	0.058	0.107	0.051	0.037	0.050
Mn	0.000	0.001	0.000	0.000	0.000
Mg	0.009	0.086	0.003	0.004	0.013
Ca	0.923	0.863	0.931	0.905	0.927
Sr	0.005	0.007	0.004	0.022	0.004
Na	0.016	0.018	0.016	0.032	0.017
Cation sum	2.021	2.062	2.018	2.015	2.022

\* analyses made next to pectolite.

Sm–Nd and Rb–Sr isotopic analysis was performed on aphanitic and macrocrystal monticellite–serpentine phlogopite kimberlites. In general terms, these samples show similar Nd–Sr isotopic characteristics (Table 7), with moderate Rb and high Sr abundances and a range of <sup>87</sup>Rb/<sup>86</sup>Sr between 0.30 and 0.72. The calculated initial <sup>87</sup>Rb/<sup>86</sup>Sr ratios show a small range from 0.7037 ±

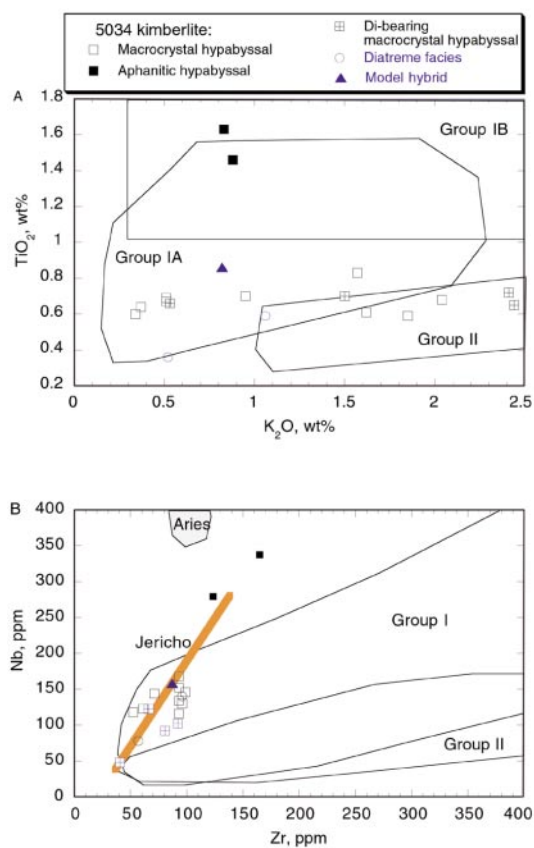


FIG. 7. Bulk chemical compositions of the 5034 kimberlite: TiO<sub>2</sub> versus K<sub>2</sub>O (A), Nb versus Zr (B). Also shown are compositional fields for Group I, Group IA, Group IB, and Group II kimberlites (Taylor *et al.* 1994); updated with new data of Mitchell (1995), O'Brien & Tyni (1999), Coe *et al.* (2003), for the Aries kimberlite (Taylor *et al.* 1994), and the Jericho kimberlite (light grey line, Kopylova *et al.* 1998). Here and below, the model hybrid kimberlite (Table 1) is calculated as a mixture of the primary kimberlitic magma with mantle and crustal material. Here and on Figure 8, the 5034 macrocrystal diopside-free kimberlite include monticellite – phlogopite – serpentine kimberlite and phlogopite – serpentine kimberlite, whereas macrocrystal diopside-bearing kimberlite include all varieties of diopside-bearing kimberlite (with or without melilite and monticellite).

TABLE 6. BULK COMPOSITIONS OF THE 5034 KIMBERLITE

Sample No	61- K2	15- K1A	15- K1	21- K2	48- K1	AK 2066	AK 2Q171	AK2 E138	AK2 E179	AK2 E466	AK2 E347	AK2 N208	AK2 Q96	11- 5KDA	11- 5KDB	8- K4A	8- K4B
JMT	M	M	M	M	M	M	M	M	M	M	M	T	T	M	M	M	M
Description	MDM	A	MD	M	A	M	M	M	M	M	M			PS	PS	MD	MD
SiO <sub>2</sub> wt. %	41.21	34.44	37.25	37.22	35.15	37.79	36.31	39.93	38.86	38.38	36.93	41.33	44.56	41.87	39.68	39.93	40.21
TiO <sub>2</sub>	0.70	1.63	0.66	0.83	1.46	0.70	0.60	0.59	0.61	0.68	0.67	0.59	0.36	0.69	0.64	0.65	0.72
Al <sub>2</sub> O <sub>3</sub>	2.73	4.25	2.54	2.98	4.31	2.94	3.04	3.45	3.63	3.57	2.69	3.83	1.93	1.84	1.51	3.28	3.58
Cr <sub>2</sub> O <sub>3</sub>	0.26	0.51	0.26	0.26	0.49	0.32	0.26	0.23	0.25	0.25	0.29	0.23	0.15	0.26	0.25	0.22	0.23
Fe <sub>2</sub> O <sub>3</sub>	3.59	4.60	3.44	3.49	4.92	4.18	3.87	3.87	3.81	3.77	2.73	3.25	2.12	4.24	4.26	3.31	3.30
FeO	4.96	5.01	4.86	5.08	4.41	3.91	3.12	3.20	3.53	4.07	5.45	3.54	3.04	2.11	2.14	4.63	4.84
MnO	0.13	0.24	0.15	0.16	0.20	0.12	0.13	0.14	0.13	0.14	0.15	0.10	0.07	0.09	0.09	0.14	0.14
MgO	34.17	27.49	35.77	35.04	28.30	32.06	34.52	26.96	30.61	32.04	34.69	30.42	34.06	31.13	31.69	32.29	31.40
CaO	3.38	5.45	2.02	6.04	8.76	1.50	0.84	5.79	3.71	3.22	7.38	1.43	0.45	2.96	4.18	4.73	4.97
Na <sub>2</sub> O	0.25	0.28	0.19	0.16	0.19	0.21	0.17	0.92	0.52	0.74	0.27	0.31	0.22	0.19	0.18	0.77	0.92
K <sub>2</sub> O	1.50	0.83	0.53	1.57	0.88	0.95	0.34	1.85	1.62	2.04	0.51	1.06	0.52	0.51	0.37	2.44	2.41
P <sub>2</sub> O <sub>5</sub>	0.16	1.14	0.52	0.36	0.41	0.30	0.41	0.38	0.38	0.37	0.49	0.34	0.23	0.30	0.27	0.35	0.37
CO <sub>2</sub>	0.70	0.95	0.33	0.37	0.29	0.81	0.70	0.44	0.40	0.62	0.77	0.22	0.26	2.00	2.90	0.60	0.40
H <sub>2</sub> O <sup>+</sup>						11.35	12.90	8.97	9.93	7.26	5.47	9.48	9.44	10.60	11.10	5.70	5.61
H <sub>2</sub> O <sup>-</sup>						1.92	2.43	1.88	1.41	1.04	0.67	2.79	1.01	0.30	0.20	<0.01	<0.01
H <sub>2</sub> O	5.87	11.87	11.09	5.59	9.61	13.27	15.33	10.85	11.34	8.30	6.14	12.27	10.45	1.64	1.66	5.70	5.61
LOI	6.57	12.82	11.42	5.96	9.90	13.60	15.74	11.37	11.85	9.47	6.85	12.55	11.04	12.90	14.20	6.12	5.92
Total	99.88	99.32	99.90	99.48	99.60	99.01	99.70	99.04	99.90	99.19	99.71	99.37	99.09	99.48	99.75	99.58	99.78
Ni ppm	1675	786	1582	1497	889									1310	1405	1310	1405
Ba	727	4709	1034	1583	801	1080	335	1150	1265	2060	2520	975	445	1290	899	1310	1485
Ce	86	369	168	186	352									112	143.5	148.5	153
Rb	67.8	93.2	56.7	119	81	68	24	94	86	120	70	74	36	30.8	23.6	102.5	102
Sr	337.8	874.2	445.1	699	712.1	214	458	514	516	2720	1715	496	316	163.5	153.5	576	634
Nb	48	337.3	122.6	143.7	279.3	152	134	116	130	168	146	140	78	123	118	92	102
Zr	40.7	164.9	66.3	71.4	123.4	93	93	93	96	93	99	96	57	61.2	52.4	80.8	92.3
Y	3	11.5	5.5	3.9	12.1	10	10	10	10	8	10	10	6	8.4	8.9	7.7	8.4
S						400	800	200	100	200	300	500	500				
Ga	3.9	3.9	3.2	3.6	4.6									8	8	7	7
Pb	4.1	25.3	10.3	9.7	14.6									6	<5	12	14
Th	8.9	34.1	15.8	21	39									17	16	13	14
U	3.9	12.3	4.1	8.3	9.6									3.1	2.9	2.2	2.4
Contam. Index	1.189	1.337	1.086	1.057	1.319	1.206	1.123	1.445	1.271	1.182	1.117	1.397	1.331	1.365	1.276	1.183	1.234
Mg#	88.2	84.4	89.0	88.5	85.2	88.3	90.4	87.9	88.8	88.5	88.8	89.4	92.5	90.4	90.5	88.4	87.8

JMT: juvenile magma texture; M: magmatic in hypabyssal kimberlite, T: tuffisitic in diatreme-facies kimberlite.

Description: M: macrocrystal monticellite–phlogopite–serpentine kimberlite, MD: macrocrystal diopside-bearing; MDM: macrocrystal diopside- and melilitite-bearing, A: aphanitic, PS: macrocrystal phlogopite–serpentine kimberlite.

Analytical results for the AK kimberlites were provided by Canamera Geological Ltd. (courtesy of H. Cookenboo).

Where H<sub>2</sub>O and H<sub>2</sub>O<sup>-</sup> are reported, H<sub>2</sub>O<sup>+</sup> was determined at 105°C, and H<sub>2</sub>O<sup>-</sup> was calculated by difference between LOI, CO<sub>2</sub> and H<sub>2</sub>O<sup>+</sup>.

0.0003 to  $0.7040 \pm 0.0001$  (Table 7;  $\epsilon\text{Sr}_T -2$  to  $+2$ ). The two aphanitic samples (48–K1A, 15–K1A) have the highest Sr contents, and lowest Rb/Sr values. The abundances of Sm and Nd are high, and the  $^{147}\text{Sm}/^{144}\text{Nd}$  values are very low, reflecting the steeply LREE-enriched nature of the kimberlite, and show a very small range, from 0.0774 to 0.0778. This total range ( $\pm 0.0002$ ) is identical to the reproducibility of  $^{147}\text{Sm}/^{144}\text{Nd}$  for the standards monitored, such as BCR–1. Similarly, variations in the Nd isotopic composition

between samples are very small, ranging from  $\epsilon\text{Nd}_T$  values of 0.0 to  $+0.9$ , with each analysis having an estimated uncertainty of  $\pm 0.4 \epsilon$  units. Like the  $\epsilon\text{Sr}$  isotope data, the  $\epsilon\text{Nd}$  data again indicate that the four samples are effectively within uncertainty of each other.

## DISCUSSION

*The 5034 kimberlite in comparison with other kimberlites*

The 5034 kimberlite is a Group-I kimberlite, as indicated mineralogically by the presence of monticellite, and geochemically by contents of major and minor elements and the Sr–Nd signature. On an  $\epsilon\text{Sr}$ – $\epsilon\text{Nd}$  diagram (Fig. 9), the 5034 samples clearly fall within the field of Kaapvaal Group-I kimberlites, with an asthenospheric

source for the magmas (Smith *et al.* 1985). In this respect, they seem similar to the Jurassic Contwoyto–Jericho kimberlites of the northern Slave Province, but they are considerably less evolved isotopically than the younger kimberlites from the Lac de Gras field (Dowall *et al.* 2001).

Several mineralogical traits set this kimberlite apart from most other Group-I kimberlites and are reminiscent of Group-II kimberlites. These traits relate to the presence of four minerals in the groundmass of the dominant variety of the 5034 hypabyssal kimberlite, *i.e.*,

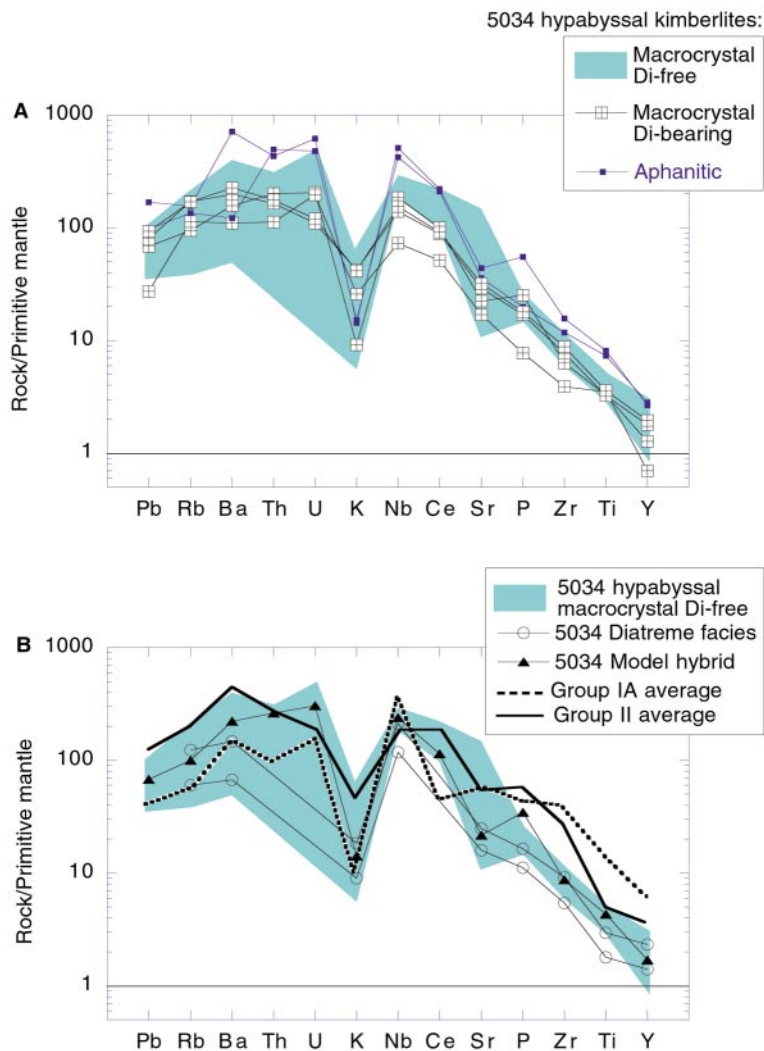


FIG. 8. Spidergrams of incompatible elements in the 5034 kimberlite normalized against primitive mantle (McDonough & Sun 1995). Patterns for Group-IA and Group-II average kimberlites are according to Smith *et al.* (1985).

TABLE 7. Rb–Sr AND Sm–Nd ISOTOPIC DATA FOR THE 5034 HYPABYSSAL KIMBERLITE

Sample	Rb ppm <sup>1</sup>	Sr ppm <sup>1</sup>	<sup>87</sup> Rb/ <sup>86</sup> Sr ID <sup>1</sup>	±2σ <sup>2</sup>	<sup>87</sup> Sr/ <sup>86</sup> Sr	±2σ <sub>m</sub> e <sup>-6</sup>	<sup>87</sup> Sr/ <sup>86</sup> Sr <sub>T</sub>	±2σ <sup>3</sup>	εSr <sub>T</sub>	<sup>143</sup> Nd/ <sup>144</sup> Nd	±2σ <sub>m</sub> e <sup>-6</sup>	εNd <sub>0</sub>	Sm ppm	Nd ppm	<sup>147</sup> Sm/ <sup>144</sup> Nd ID	εNd <sub>T</sub>
15-K1	99.7	430.1	0.6708	0.0379	0.708877	12	0.70371	0.00029	-2	0.512250	15	-7.6	8.260	64.39	0.0776	+0.7
21-K2	133.7	540.0	0.7168	0.0405	0.709373	13	0.70386	0.00031	0	0.512249	9	-7.6	7.860	61.43	0.0774	+0.7
48-K1A	77.4	710.3	0.3153	0.0178	0.706453	13	0.70403	0.00014	2	0.512218	9	-8.2	16.56	128.9	0.0777	+0.0
15-K1A	99.3	969.9	0.2962	0.0168	0.706324	15	0.70404	0.00014	2	0.512262	8	-7.3	17.00	132.1	0.0778	+0.9

1. Rb and Sr abundances and <sup>87</sup>Rb/<sup>86</sup>Sr determined by isotope dilution.
2. Uncertainty calculated by error propagation assuming ±2% uncertainty in determinations of abundances of both Rb and Sr.
3. Uncertainty calculated by error propagation using a value of ±0.00002 for <sup>87</sup>Sr/<sup>86</sup>Sr, and the calculated uncertainty for <sup>87</sup>Rb/<sup>86</sup>Sr. All values of the initial isotope ratio calculated at T = 540 Ma.

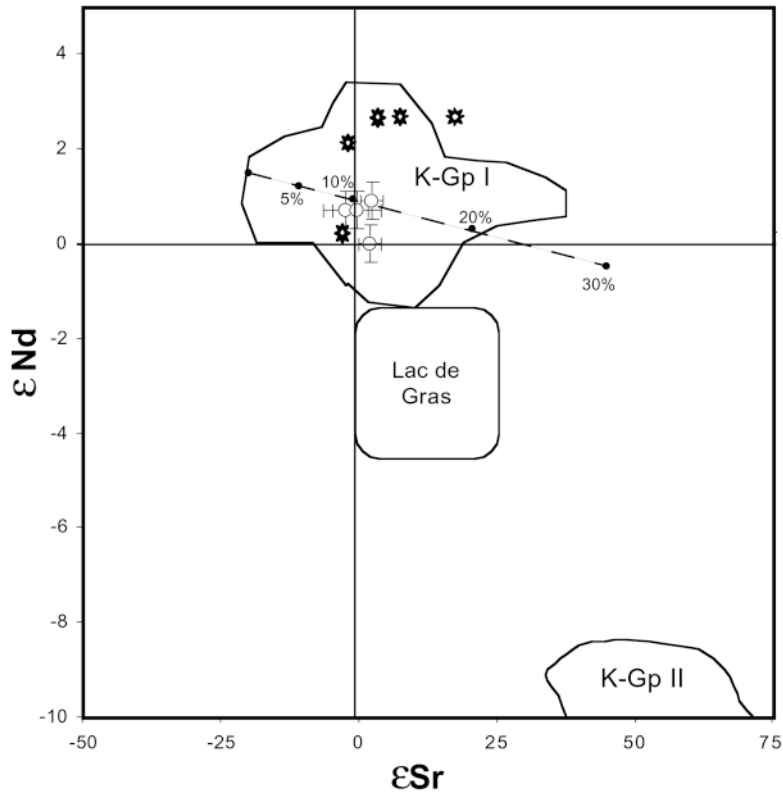


FIG. 9. εSr – εNd isotopic diagram showing the four data points of the 5034 kimberlite (open circles), which plot within the Group-I field of Kaapvaal kimberlites (Smith *et al.* 1985). The partial field of Group-II kimberlites is shown for reference. Sr–Nd data for other Slave Province kimberlites also are shown: the Jurassic Contwoyto and Jericho kimberlites (stars) and the Eocene kimberlites of the Lac de Gras field (Dowall *et al.* 2001). Also shown is a simple mixing trajectory between hypothetical primitive kimberlitic magma (εSr = -20, εNd = +1.5, Nd = 131 ppm, Sr = 840 ppm) and model Archean crust (see text for discussion). The mixing trajectory shows percentage increments of Archean crust added to a hypothetical kimberlitic magma and permit, but do not require, ~8–12% contamination of the kimberlites by Archean crust.

bright orange poikilitic phlogopite with a relatively low Al content, Cr- and Ti-rich spinel-group mineral, diopside and melilite.

Orange poikilitic phlogopite that has a relatively low content of Al, transitional to that of tetra-ferriphlogopite, is unlike the colorless Ba-enriched groundmass phlogopite common in Group-I kimberlites, and is more characteristic of Group-II kimberlites and many other rocks (Scott Smith 1996). However, a close look at the phlogopite composition reveals the unique nature of this phase in the 5034 kimberlite, as it deviates from late groundmass phlogopite in both Group-I and Group-II kimberlite. Group-I groundmass phlogopite is more aluminous, whereas Group-II groundmass phlogopite is, in general, more Al-poor (Fig. 10) and Ti-rich (5–9 wt.%  $\text{TiO}_2$ ) (Mitchell 1995). On an  $\text{Al}_2\text{O}_3$ – $\text{TiO}_2$  plot, one half of all 5034 phlogopite compositions fall outside of the Group-I and Group-II fields (worldwide database).

Figures 10 and 11 clearly illustrate the complexity and diversity of phlogopite compositions. Not only do all rock types have distinct compositional trends, but the phlogopite within a given rock-type varies significantly in composition in a manner that seems to be controlled locally by the composition of adjacent crystals. In the monticellite – serpentine – phlogopite kimberlite, phlogopite most commonly evolves continually from a tetra-ferriphlogopite (TFP) core to a phlogopite rim. This trend of a marked Al-enrichment associated with a depletion in Fe and Ti is characteristic of Group-I kimberlite (Mitchell 1995). A less common trend for phlogopite in Group-I kimberlite, a discontinuous evolution from phlogopite to tetra-ferriphlogopite, is also observed in the 5034 samples. It is represented by discrete mantles of Fe-rich phlogopite in diopside- and

monticellite-bearing kimberlite (Fig. 4C). The composition and evolution of phlogopite in the latest magmatic phase of the hypabyssal 5034 kimberlite differ drastically from those in the earlier batches of magma. Phlogopite in the younger serpentine – phlogopite kimberlite crystallizes in two episodes that produce early barian phlogopite and late Ba-poor mica. This trend of Ba depletion is opposite to the phlogopite–kinoshitalite trend commonly found in Group-I kimberlites. However, the Ba-depletion trend has been recognized in few Group-I kimberlites from Namibia and China (Mitchell 1995) and in the nearby Snap Lake hypabyssal kimberlite (Mogg *et al.* 2003). The concentration of Ba in early magmatic minerals cannot be explained by its common incompatible behavior in magmatic systems and may be a sign of a peculiar fluid regime or redox state. A higher oxidation state of the kimberlite containing phlogopite with Ba-rich core is evident in its higher  $\text{Fe}_2\text{O}_3/\text{FeO}$  value. The assimilation of Ba-rich xenolithic material is unlikely to control the behavior of Ba in the last phase of the 5034 magmatic kimberlite, as it does not differ in Ba content from other types of the 5034 kimberlite.

Superimposed on these three major trends are diverse, highly localized, random patterns of phlogopite evolution. Phlogopite that crystallized from granite-contaminated kimberlitic magma has distinct compositions richer in Ti and Ba than phlogopite that is distant from assimilated xenoliths. In these hybrid areas, phlogopite is overgrown by a rare tetra-ferriphlogopite rim next to Ca-silicates (epidote and pectolite, Fig. 5E), crystallizes a Ti- and Ba-poor mantle near strontian apatite, and develops Na-rich and Fe-poor compositions near serpentine (Fig. 5F). Furthermore, late phlogopite that

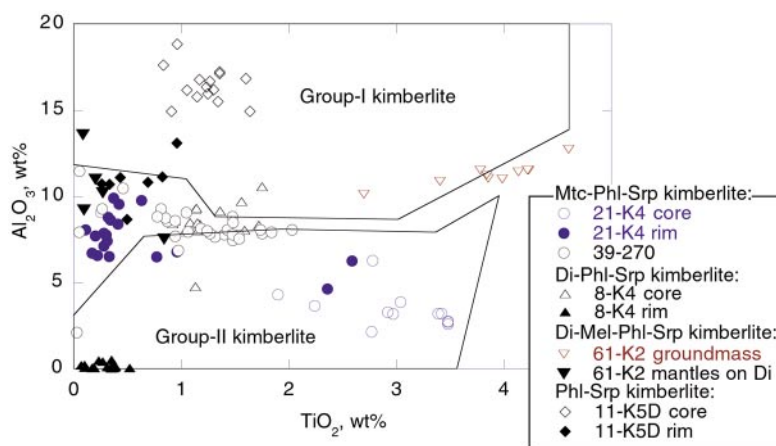


FIG. 10.  $\text{Al}_2\text{O}_3$  versus  $\text{TiO}_2$  diagram for groundmass micas in kimberlitic rocks, including 5034 kimberlite. Fields for Group-I and -II kimberlites outline analyses of groundmass micas from Mitchell (1995).

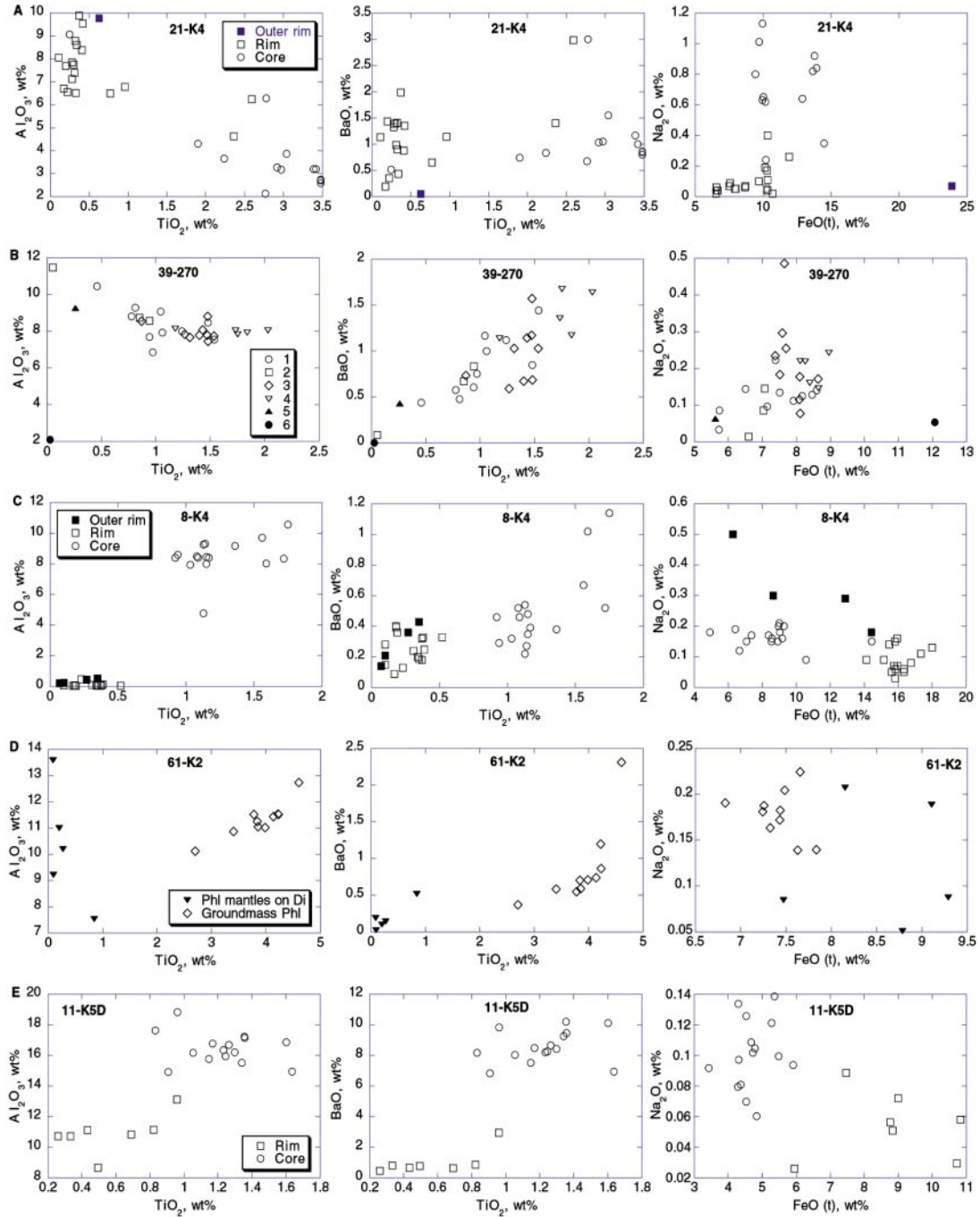


FIG. 11. Compositions of groundmass micas in the 5034 hypabyssal kimberlite on the  $Al_2O_3 - TiO_2$ ,  $BaO - TiO_2$  and  $Na_2O - FeO$  (t) plots for macrocrystal monticellite – phlogopite – serpentine kimberlite 21-K4 and 39-270 (A and B), macrocrystal diopside- and monticellite-bearing phlogopite – serpentine kimberlite 8-K4 (C), macrocrystal diopside- and melilite-bearing phlogopite – serpentine kimberlite 61-K2 (D), and macrocrystal phlogopite – serpentine kimberlite 11-K5D (E). Symbols for sample 39-270 designate phlogopite compositions of core in zoned grains (1), rim in zoned grains (2), homogeneous grains (3), grains in areas of assimilated felsic material (4), grain in contact with strontian apatite (5), and grain in contact with pectolite (6).

mantles groundmass diopside is distinct from earlier poikilitic phlogopite in being Fe-rich and Ti-poor. These observations suggest that the major disequilibrium between locally (~20  $\mu\text{m}$ ) buffered areas is due to extreme quenching and uneven contamination. Overall, the residual, highly contaminated magma tends to precipitate Fe-rich and Ti-poor phlogopite. The large variability of phlogopite compositions in the 5034 hypabyssal kimberlite is due to very local diffusion-controlled crystallization, and not to changes in the bulk composition of the magma. If kinetic factors such as the rate of transport of cations to the growing crystals, the availability of the cations in the proximity of the growing crystal, and the local degree of undercooling control phlogopite compositions, their role as petrogenetic indicators of changing bulk-composition of the melt (Mitchell 1995) needs to be re-evaluated.

Similar to phlogopite, the groundmass spinel-group mineral also shows compositions intermediate between those of Group-I and Group-II kimberlite. Spinel in Group-I kimberlite is characterized by decreasing Cr/(Cr + Al) ratio with increasing Ti, but Group-I kimberlites that have crystallized abundant phlogopite prior to spinel crystallization commonly have spinel that falls on the Group-II kimberlite trend (Mitchell 1995). On the Ti–Cr diagram (Fig. 6B), the 5034 spinel-group minerals plot on the trend diagnostic of spinel minerals in Group-II kimberlite. However, the Fe content of the 5034 spinel-group mineral is intermediate between the high values encountered in Group-II kimberlite and the much lower Fe/(Fe + Mg) values encountered in the Group-I kimberlite (Fig. 6A).

#### *Effects of contamination by granitic xenoliths*

Contamination by felsic material affected many traits of the 5034 hypabyssal magma. This “digested” material manifests itself as areas unusually rich in non-poikilitic phlogopite, pectolite, epidote, calcite, serpentine, barite and melilite, and atypically poor in spinel-group minerals, monticellite and chlorite–serpentine. Patches of similar mineralogy and texture (radiating pectolite, abundant phlogopite, carbonate and serpentine) were described as “kimberlitized” crustal xenoliths in South African kimberlites (Scott Smith *et al.* 1983). The presence of groundmass pectolite inevitably records partial or total digestion of xenolithic material by the kimberlitic magma (Scott Smith *et al.* 1983). Early and extensive assimilation of Na-rich xenoliths by kimberlitic magma leads to atypical high Na content in the melt, which results in the crystallization of pectolite from the residual fluid at low temperatures as a pseudo-primary groundmass mineral. Formation of diopside in Group-I kimberlite is also ascribed to its contamination by either partly or totally digested country-rock (Mitchell 1995). All diopside in the 5034 kimberlite may be pseudo-primary, as compositions of the groundmass diopside and the corona diopside are

identical. Diopside and phlogopite are strongly associated in reaction coronas on xenoliths; phlogopite and diopside are jointly absent from the 5034 aphanitic kimberlite. Much of the phlogopite can thus be regarded as pseudo-primary or hybrid in the kimberlite.

We contend that the apparent affinity of the 5034 kimberlite to Group-II kimberlites may well stem from its increased Si content due to contamination by granite. This contamination increases the Contamination Index (compare CI values of the parental magma and hybrid kimberlite rock in Table 1), but does not necessarily make its value very high and indicative of contaminated kimberlites (CI = 1.5; Mitchell 1986). This example illustrates the importance of detailed petrographic work for the correct classification of kimberlites. Mineralogically unusual Group-I kimberlites should be carefully checked for subtle signs of contamination by felsic material before larger-scale constraints on their origin are assessed (Taylor & Kingdom 1999).

The assimilation began after the magma had started its groundmass crystallization, but at relatively high temperatures, as suggested by the development of distinct disequilibrium assemblages of minerals at the latest stages of crystallization from a residual highly contaminated melt. Mantles of distinct phlogopite with relatively high Fe<sup>2+</sup> or Na contents and strontian perovskite record this shift in the groundmass mineralogy. The high temperatures of the assimilation are evident by the crystallization of diopside, a relatively high-T mineral, from hybrid magma. Diopside formed early, as it is commonly included in poikilitic phlogopite. The temperatures at which clinopyroxene begins to crystallize from a Group-I kimberlitic magma with  $X(\text{CO}_2) = 0.24$  could be as high as 1200°C at 10 kbar (Edgar *et al.* 1988). At T = 950°C and 15 kbar, clinopyroxene crystallizes from olivine lamproite with H<sub>2</sub>O  $\gg$  CH<sub>4</sub> (Foley 1990). The temperatures will be lower for crystallization of the clinopyroxene in the groundmass of hypabyssal kimberlites at subsurface conditions (P  $\approx$  1 kbar).

The assimilation of granitic material in tuffitic breccias was inhibited by severe quenching and slow diffusion due to loss of volatiles in an explosive emplacement.

#### *Model of contamination*

The primitive initial Sr–Nd isotopic ratios of the 5034 kimberlite constrain the amount of granitic material that could have been incorporated into the host magma. We modeled the Nd–Sr systematics of such an assimilation process. Considerable Nd isotopic data are available for granitic rocks of the Slave Province (Yamashita *et al.* 1999, Davis & Hegner 1992). We used the Nd isotope data of Yamashita *et al.* (1999) from regional late Archean granites of the southern Slave Province to evaluate the contamination process. At 540 Ma, the age of intrusion of the 5034 pipes, the data of

Yamashita *et al.* (1999) yield an average  $\epsilon\text{Nd}$  value of  $-19.5$  and an average Nd abundance of 32 ppm for southern Slave Province Archean granites. Modeling of Sr isotope variations is more problematic, as the Sr isotope data for the Archean rocks of the Slave province are not readily available. For this purpose, we assumed that late Archean crust has an average  $^{87}\text{Sr}/^{86}\text{Sr}$  ratio of 0.705. Using the average Rb and Sr abundances of the upper crust of Taylor & McLennan (1985), we calculate that at 540 Ma, this crust would have a  $^{87}\text{Sr}/^{86}\text{Sr}$  of 0.7327 ( $\epsilon\text{Sr} = 410$ ). We use these data together with a simple mixing model (Gray 1984) to evaluate the degree of potential assimilation allowed by the isotope data for kimberlite. Given that the four 5034 samples analyzed have basically identical  $\epsilon\text{Sr}$ – $\epsilon\text{Nd}$  values, we model a hypothetical kimberlitic magma with  $\epsilon\text{Sr}$ – $\epsilon\text{Nd}$  values at the primitive edge of the Kaapvaal Group-I field ( $\epsilon\text{Sr} = -20$ ,  $\epsilon\text{Nd} = +1.5$ , Fig. 9), and add model Archean crust as described above by simple mixing. The Nd and Sr abundances of the hypothetical primitive magma were chosen to be the average of samples 15–K1A and 48–K1A (Nd = 131 ppm, Sr = 840 ppm), as these are mineralogically the least-contaminated samples. The results of this modeling are presented in Figure 9 and show that between ~8 and 12% Archean crust is permitted to have been incorporated in the analyzed 5034 kimberlites, based on the  $\epsilon\text{Sr}$ – $\epsilon\text{Nd}$  relationships alone.

The next step in modeling the composition of the 5034 hypabyssal kimberlite was assessing the bulk composition of the hybrid rock (Table 1). An aphanitic kimberlite poor in diopside and phlogopite was taken as the best estimate of the parental uncontaminated kimberlitic magma. An average southeastern Slave granite (Table 1) was considered representative of the crustal contaminant. Disaggregation of garnet peridotite accounted for the presence of 30% of the mantle-derived xenocrystic olivine in the hybrid kimberlite. The resulting estimate of the bulk composition of the contaminated kimberlite has a significantly higher  $\text{SiO}_2$  and MgO than that of the parental magma (Table 1, Fig. 12) and is close to the analyzed macrocrystal 5034 kimberlite with respect to all chemical parameters (Figs. 7, 8). Disaggregation of ~30–40% garnet peridotite into a kimberlitic magma contaminated by crust has no significant effect on the  $\epsilon\text{Sr}$ – $\epsilon\text{Nd}$  systematics, because the Sr and Nd abundances in peridotite are very low, and those in kimberlite very high. More than 90% addition of typical peridotite would be required to significantly alter the  $\epsilon\text{Sr}$ – $\epsilon\text{Nd}$  systematics.

#### On melilite in kimberlite

A totally serpentinized mineral that occurs in long laths together with diopside in the hypabyssal 5034 kimberlite could be either phlogopite, calcite, or melilite. We interpreted the mineral as melilite on the basis of the following petrographic observations. Rect-

angular terminations of the grains are uncharacteristic of calcite. The mineral is serpentinized, whereas primary calcite in kimberlites is typically replaced by secondary calcite, and phlogopite is fresh in the 5034 samples. The mineral is found only in areas that assimilated granitic xenoliths. These areas are relatively enriched in Si (Fig. 12), and it is where one would expect to see crystallization of high-Si (relative to olivine and monticellite) melilite, not the Si-free calcite.

Melilite occasionally occurs in kimberlites (Mahotkin *et al.* 2003, Skinner *et al.* 1999, Scott Smith 1989, Murthy *et al.* 1994, Egorov 1979), but rocks with abundant (>10 vol.%) melilite should not be classified as kimberlites (Mitchell 1986, Woolley *et al.* 1996). Experimental studies of near-solidus melts produced at 30 kbar (Gudfinnsson & Presnall 2003) and at 30–70 kbar in the carbonated mantle peridotite (Canil & Scarfe 1990) suggest that it may be possible to generate a continuous spectrum of partial melts varying in composi-

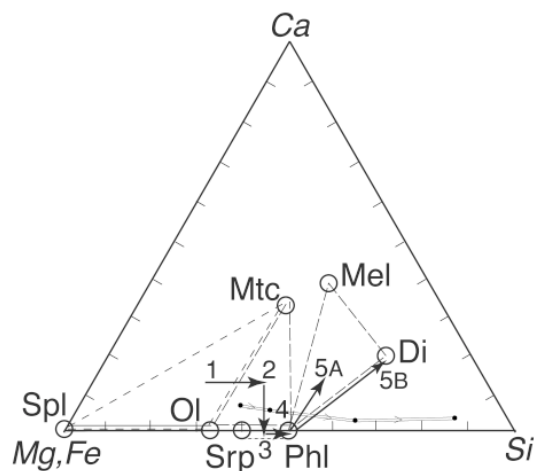


FIG. 12. Common minerals of the kimberlites in a Mg, Fe – Ca – Si (moles) plot. Patterning lines indicate mineral parageneses of the 5034 hypabyssal kimberlite corresponding to progressively higher contamination by granite: 1: uncontaminated groundmass of aphanitic kimberlite (Spl + Mtc + Ol); 2: macrocrystal kimberlite (Ol + Mtc + Phl + Srp + Spl); 3: a wide outer zone of serpentinization around granite inclusions (Srp + Phl); 4: zone of monomineralic phlogopite in coronas on granite inclusions (Phl); 5A: patches replacing totally digested granite xenoliths (Mel + Phl + Di); 5B: inner zone of monomineralic diopside in coronas on granite inclusions (Di). Positions of points 1–5 inside paragenetic triangles are arbitrary and do not correspond to actual mineral modes. Small black points connected by double lines with arrows indicate the change in whole-rock compositions from aphanitic uncontaminated kimberlite to hybrid kimberlite, then to serpentinized granite xenolith and to fresh SE Slave granite (all compositions are from Table 1, and are recalculated to molar amounts).

tion from kimberlite to melilitite. Pseudomorphs after melilite are present in most Group-II kimberlite and in some phlogopite-rich Group-I kimberlites, and are more common in the diatreme facies than in the hypabyssal kimberlites (Skinner *et al.* 1999). Melilite in kimberlites is associated with diopside and phlogopite, but shows a strong negative connection to monticellite (Skinner *et al.* 1999). Experimental data on the stability of melilite in potassium-rich magmas (Yoder 1986 and references therein) were used to constrain conditions of its crystallization.

The presence of melilite in kimberlitic magmas has been explained by several hypotheses. The first of these emphasizes pressure and temperature controls on the stability field of melilite (Moore 1983). As melilite is unstable at  $P > 9$  kbar and at  $T < 900^\circ\text{C}$  in  $\text{CO}_2$ -saturated conditions, it can only crystallize from a relatively high- $T$  magma, but would not commonly crystallize in kimberlites with low ( $\sim 350^\circ\text{C}$ ) temperatures of emplacement (Moore 1983). The second hypothesis ties the crystallization of melilite to  $\text{CO}_2$  loss due to degassing of kimberlitic magma (Skinner *et al.* 1999). The third model points out that melilite should crystallize from a kimberlitic magma with higher  $\text{SiO}_2$  content (Skinner *et al.* 1999) on the basis of mineral-compatibility diagrams for K-rich ultrabasic magmas at 3 kbar and  $1000^\circ\text{C}$  (Yoder 1986). As the bulk composition of K-rich rocks becomes progressively Si-rich, they should crystallize the assemblage olivine + phlogopite + melilite instead of monticellite + olivine + phlogopite.

Our observations suggest that the presence of melilite in the 5034 kimberlite is controlled by the bulk composition of the magma, particularly its high Si activity, therefore supporting the latter hypothesis. Although all samples of hypabyssal 5034 kimberlite crystallized at similar pressures and temperatures, melilite and diopside in many samples are restricted to the reaction rim around granitic xenoliths. The pressure-temperature control on crystallization of melilite is thus negligible.

The development of a mineralogically zoned reaction rim on granitic xenoliths records sharp increases in Si activity near the inclusions. It is evident in the trend of whole-rock compositions as it changes from aphanitic kimberlite to model hybrid kimberlite, and then to serpentinized and fresh granite (Fig. 12). This increase led to changes in mineral assemblage from olivine + monticellite + spinel + phlogopite in the host kimberlite to serpentine + spinel + phlogopite closer to the granite inclusions (Fig. 4A), then to phlogopite (Phl), and lastly to diopside (Di) in the inner parts of the reaction corona (Fig. 4C). The diffusion of Si into the host magma led to the replacement of olivine and monticellite by serpentine, then by phlogopite and diopside, in full correspondence with the increasing Si activity and  $\text{Si}/(\text{Fe} + \text{Mg})$  values in these minerals (Fig. 12). The plot explains a strong positive connection of melilite and diopside and the occurrence of melilite only in diopside-bearing 5034

kimberlite. This progression of mineral assemblages also explains the incompatibility between the Si-poor monticellite and the Si-rich diopside. Not only do they never occur within one zone of the reaction rims on the granitic xenoliths, but monticellite is much rarer and completely altered in diopside-bearing 5034 kimberlite. Our observations conform to a trend of mutual exclusion of monticellite and diopside in kimberlites (Mitchell 1995).

The fact that melilite is more common in the diatreme facies than in hypabyssal kimberlites led to a proposed  $\text{CO}_2$  control on the melilite crystallization (Skinner *et al.* 1999), but the distribution can also be explained on the basis of local Si activity of the magma. When magma degasses, the activity of all remaining components increases. Si activity increases most, as it is the most abundant component of the magma. The relative Si enrichment of degassed magma results in crystallization of diopside growing upon lapilli in diatreme-facies kimberlites (Scott Smith 1996) and could also cause the crystallization of melilite.

#### CONCLUSIONS

1. Kimberlite 5034 of the Gahcho Kue cluster of the southeastern Slave craton is a multiphase intrusion composed of the pyroclastic diatreme facies kimberlite and magmatic hypabyssal kimberlite. The kimberlitic magma with Group-I affinity originated in the deep asthenosphere and intruded into Archean granitic material that variously contaminated several consecutive batches of kimberlitic magma. At least four different phases of magmatic activity are recognized. Aphanitic monticellite-serpentine kimberlite formed early and contemporaneously with respect to the main hypabyssal phase magmas and is present in autoliths and cross-cutting dikes. The dominant hypabyssal phase is composed of macrocrystal monticellite - phlogopite - serpentine kimberlite. The subsequent explosive magmatic phase formed tuffisitic kimberlite breccia. The final batch of kimberlitic magma was drastically different from preceding melts in its  $\text{Fe}_2\text{O}_3/\text{FeO}$  value and crystallized barian phlogopite with an atypical trend of chemical evolution.

2. The macrocrystal monticellite - phlogopite - serpentine kimberlite assimilated significant amount of granitic xenoliths, which caused crystallization of pseudo-primary phlogopite, diopside, melilite and pectolite from a hybrid melt enriched in Si and Na. The mineralogical character of the 5034 kimberlite, which is intermediate between Group-I and Group-II kimberlites, can be explained by its strong contamination by crust. The shift in bulk composition of the magma due to the addition of granitic material is likely to have occurred at relatively high temperatures. The  $\epsilon\text{Sr}-\epsilon\text{Nd}$  systematics of the 5034 kimberlite are primitive and permit incorporation of 8-12% Archean granites. The bulk composition of the macrocrystal 5034 kimberlite

can be modeled by the addition of 38% mantle peridotite and 10% granite to the parental magma, approximated by the aphanitic kimberlite.

3. All recognized hypabyssal rock-types have distinct compositional trends of phlogopite, but phlogopite within a given rock-type also varies significantly in response to local chemical heterogeneities and the composition of proximal minerals. Areas of assimilated felsic material crystallized Ti- and Ba-rich phlogopite and Sr-rich apatite. The large variability of phlogopite composition in the 5034 hypabyssal kimberlite is due to very local diffusion-controlled crystallization, and not to changes in bulk composition of the magma.

#### ACKNOWLEDGEMENTS

We thank H. Grutter and B. Scott Smith for discussions on various aspects of the study, and C. Hetman and B. Wyatt for providing geological information on the samples. Harrison Cookenboo and Canamera Geological Ltd. are thanked for making available bulk-chemical analyses of the GK kimberlite. We are indebted to an anonymous reviewer and R.F. Martin for comments on the manuscript, and to De Beers Canada and Mountain Province Ltd. for permission to publish the results. Funding for this research derived from NSERC research grant to MGK (2000–current). The Radiogenic Isotope Facility at the University of Alberta is supported, in part, by an NSERC Major Facilities Access Grant.

#### REFERENCES

- BETHUNE, K.M., VILLENEUVE, M.E. & BLEEKER, W. (1999): Laser  $^{40}\text{Ar}/^{39}\text{Ar}$  thermochronology of Archean rocks in Yellowknife domain, southwestern Slave Province: insights into the cooling history of an Archean granite–greenstone terrane. *Can. J. Earth Sci.* **36**, 1189–1206.
- CAIRNS, S.R., MACLACHLAN, K., RELF, C., RENAUD, J. & DAVIS, W.J. (2003): Digital atlas of the Walmsley Lake area, NTS 75N. *C.S. Lord Open File* **2003–04**.
- CANIL, D. & SCARFE, C.M. (1990): Phase relations in peridotite +  $\text{CO}_2$  systems to 12 GPa: implications for the origin of kimberlite and carbonate stability in the Earth's upper mantle. *J. Geophys. Res.* **95**, B15805–15816.
- COE, N., LE ROUX, A. & GURNEY, J. (2003): The petrology and geochemistry of the Swartruggens and Star kimberlite dyke swarms, South Africa. *Eighth Int. Kimberlite Conf. (Victoria), Extended Abstr. Vol.*
- CREASER, R.A., ERDMER, P., STEVENS, R.A. & GRANT, S.L. (1997): Tectonic affinity of the Nisutlin and Anvil assemblage strata from the Teslin tectonic zone, northern Canadian Cordillera: constraints from neodymium isotope and geochemical evidence. *Tectonics* **16**, 107–121.
- DAVIS, W.J. & HEGNER, E. (1992): Neodymium isotopic evidence for the tectonic assembly of late Archean crust in the Slave Province, northwest Canada. *Contrib. Mineral. Petrol.* **111**, 493–504.
- DOWALL, D.P., NOWELL, G.M., PEARSON, D.G., KJARSGAARD, B.A. & KOPYLOVA, M.G. (2001): Comparative geochemistry of the source regions of southern African and Slave kimberlites. *Slave–Kaapvaal Workshop 2001, Abstr. Vol.*
- EDGAR, A.D., ARIMA, M., BALDWIN, D.K., BELL, D.R., SHEE, S.R., SKINNER, E.M.W. & WALKER, E.C. (1988): High-pressure – high-temperature melting experiments on a  $\text{SiO}_2$ -poor aphanitic kimberlite from the Wesselton mine, Kimberley, South Africa. *Am. Mineral.* **73**, 524–533.
- EDWARDS, D., ROCK, N.M.S., TAYLOR, W.R., GRIFFIN, B.J. & RAMSAY, R.R. (1992): Mineralogy and petrology of the Aries diamondiferous kimberlite pipe, central Kimberley block, Western Australia. *J. Petrol.* **33**, 1157–1191.
- EGOROV, K.N. (1979): On the find of melilite in kimberlite pipe “Udachanya-Eastern”. *Dokl. Acad. Nauk SSSR* **248**(4), 949–952 (in Russ.).
- FIELD, M. & SCOTT SMITH, B. (1999): Contrasting geology and near-surface emplacement of kimberlite pipes in Southern Africa and Canada. *In Proc. Seventh Int. Kimberlite Conf. (J.J. Gurney et al., eds.)*. Red Roof Designs, Cape Town, South Africa (214–237).
- FOLEY, S.F. (1990): A review and assessment of experiments on kimberlites, lamproites and lamprophyres as a guide to their origin. *Proc. Indian Acad. Sci. (Earth Planet. Sci.)* **99**(1), 57–80.
- GRAY, C.M. (1984): An isotopic mixing model for the origin of granitic rocks in southeastern Australia. *Earth Planet. Sci. Lett.* **70**, 47–60.
- GUDFFINSON, G.H. & PRESNALL, D.C. (2003): Continuous gradations among primary kimberlitic, carbonatitic, melilititic, and komatiitic melts in equilibrium with garnet lherzolite at 3–8 GPa. *Eighth Int. Kimberlite Conf. (Victoria), Extended Abstr. Vol.*
- HEAMAN, L.M., KJARSGAARD, B. & CREASER, R.A. (2003): The timing of kimberlite magmatism in North America: implications for global kimberlite genesis and diamond exploration. *Lithos* **71**(2–4), 153–184.
- HETMAN, C.M., SCOTT SMITH, B.H., PAUL, J.L. & WINTER, F.W. (2003): Geology of the Gahcho Kue kimberlite pipes, NWT, Canada: root to diatreme transition zones. *Eighth Int. Kimberlite Conf. (Victoria), Extended Abstr. Vol.*
- HOLMDEN, C., CREASER, R.A., MUEHLENBACHS, K., BERGSTROM, S.M. & LESLIE, S.A. (1996): Isotopic and elemental systematics of Sr and Nd in 454 Ma biogenic apatites: implications for paleoseawater studies. *Earth Planet. Sci. Lett.* **142**, 425–437.
- KOPYLOVA, M.G. & CARO, G. (2004): Mantle xenoliths from the southeastern Slave craton: evidence for chemical zona-

- tion in a thick cold lithosphere. *J. Petrol.* (in press).
- \_\_\_\_\_, RUSSELL, J.K. & COOKENBOO, H. (1998): Petrography and chemistry of the Jericho kimberlite (Slave Craton, northern Canada). *In Proc. Seventh Int. Kimberlite Conf.* (J.J. Gurney *et al.*, eds.). Red Roof Designs, Cape Town, South Africa (449-451).
- KRETZ, R. (1983): Symbols for rock-forming minerals. *Am. Mineral.* **68**, 277-279.
- MAHOTKIN, I., ROBEY, J., KURSZLAUKIS, S., VALUEV, E. & PYLAEV, N. (2003): Pipe emplacement model of the Lomonosov diamond deposit, Archangelsk region, NW Russia. *Eighth Int. Kimberlite Conf. (Victoria), Ext. Abstr. Vol.*
- MCDONOUGH, W.F. & SUN, S. S. (1995): The composition of the Earth. *Chem. Geol.* **120**, 223-253.
- MITCHELL, R.H. (1986): *Kimberlites: Mineralogy, Geochemistry, and Petrology*. Plenum Press, New York, N.Y.
- \_\_\_\_\_. (1995): *Kimberlites, Orangeites, and Related Rocks*. Plenum Press, New York, N.Y.
- MOGG, T., KOPYLOVA, M.G., SCOTT SMITH, B. & KIRKLEY, M. (2003): Petrology of the Snap Lake kimberlite, NWT, Canada. *Eighth Kimberlite Conf. (Victoria), Ext. Abstr. Vol.*
- MOORE, A.E. (1983): A note on the occurrence of melilite in kimberlites and olivine melilitites. *Mineral. Mag.* **47**, 404-406.
- MURTHY, D.S.N., DAYAL, A.M. & NATARJAN, R. (1994): Mineralogy and geochemistry of Chigicherla kimberlite and its xenoliths, Anapur district, South India. *J. Geol. Soc. India* **43**, 329-341.
- O'BRIEN, H.E. & TYNI, M. (1999): Mineralogy and geochemistry of kimberlites and related rocks from Finland. *In Proc. Seventh Int. Kimberlite Conf.* (J.J. Gurney *et al.*, eds.). Red Roof Designs, Cape Town, South Africa (625-636).
- RIKHOTSO, C.T., PONIATOWSKI, B.T. & HETMAN, C.M. (2003): Overview of the exploration, evaluation, and geology of the Gahcho Kue kimberlites, Northwest Territories. *In Eighth Int. Kimberlite Conf., Slave Province and Northern Alberta Field Trip Guidebook* (B.B. Kjarsgaard, ed.). *Geol. Surv. Can.*, 79-86.
- SCOTT SMITH, B.H. (1989): Lamproites and kimberlites in India. *Neues Jahrbuch Mineral., Abh.* **161**, 193-225.
- \_\_\_\_\_. (1996): Kimberlites. *In Undersaturated Alkaline Rocks: Mineralogy, Petrogenesis, and Economic Potential* (R.H. Mitchell, ed.). *Mineral. Assoc. Can., Short Course Vol.* **24**, 217-242.
- \_\_\_\_\_, SKINNER, E.M.W. & CLEMENT, C.R. (1983): Further data on the occurrence of pectolite in kimberlite. *Mineral. Mag.* **47**, 75-78.
- SKINNER, E.M.W., MAHOTKIN, I.L. & GRUTTER, H.S. (1999): Melilite in kimberlites. *In Proc. Seventh Int. Kimberlite Conf.* (J.J. Gurney & S.R. Richardson, eds.). Red Roof Designs, Cape Town, South Africa (788-793).
- SMITH, C.B., GURNEY, J.J., SKINNER, E.M.W., CLEMENT, C.R. & EBRAHIM, N. (1985): Geochemical character of southern African kimberlites: a new approach based on isotopic constraints. *Trans. Geol. Soc. S. Afr.* **88**, 267-280.
- TANAKA, T., TOGASHI, S., KAMIOKA, H., AMAKAWA, H., KAGAMI, H., HAMAMOTO, T., YUHARA, M., ORIHASHI, Y., YONEDA, S., SHIMIZU, H., KUNIMARU, T., TAKAHASHI, K., YANAGI, T., NAKANO, T., FUJIMAKI, K., SHINJO, R., ASAHARA, Y., TANIMIZU, M. & DRAGUSANU, C. (2000): JNd-1: a neodymium isotopic reference in consistency with LaJolla neodymium. *Chem. Geol.* **168**, 279-281.
- TAYLOR, S.R. & MCLENNAN, S.M. (1985): *The Continental Crust: its Composition and Evolution*. Blackwell, Oxford, U.K.
- TAYLOR, W.R. & KINGDOM, L. (1999): Mineralogy of the Jagersfontein kimberlite – an unusual group I micaceous kimberlite – and a comment on robustness of the mineralogical definition of “orangeite”. *In Proc. Seventh Int. Kimberlite Conf.* (J.J. Gurney *et al.*, eds.). Red Roof Designs, Cape Town, South Africa (861-866).
- \_\_\_\_\_, TOMPKINS, L.A. & HAGGERTY, S.E. (1994). Comparative geochemistry of West African kimberlites: evidence for a micaceous kimberlite endmember of sublithospheric origin. *Geochim. Cosmochim. Acta* **58**, 4017-4037.
- WOOLLEY, A.R., BERGMAN, S.C., EDGAR, A.D., LE BAS, M.J., MITCHELL, R.H., ROCK, N.M.S. & SCOTT SMITH, B.H. (1996). Classification of lamprophyres, lamproites, kimberlites and the kalsilitic, melilitic, and leucitic rocks. *Can. Mineral.* **34**, 175-186.
- YAMASHITA, K., CREASER, R.A., STEMLER, J.U. & ZIMARO, T.W. (1999): Geochemical and Nd-Pb isotopic systematics of late Archean granitoids, southwestern Slave Province, Canada: constraints for granitoid origin and crustal isotopic structure. *Can. J. Earth Sci.* **36**, 1131-1147.
- YODER, H.S., JR. (1986): Potassium-rich rocks: phase analysis and heteromorphic relations. *J. Petrol.* **27**, 1215-1228.

Received March 25, 2003, revised manuscript accepted February 1, 2004.

## APPENDIX: THE COMPOSITIONS OF PHLOGOPITE

### *Macrocrystal monticellite – serpentine – phlogopite kimberlite*

In sample 21–K4, phlogopite crystals are most commonly zoned from TFP cores to phlogopite rims. This main chemical trend involves a continuous Fe-, Ba- and Ti-depletion and an Al-enrichment. Cr contents are typically very low (<0.05 wt.% Cr<sub>2</sub>O<sub>3</sub>), typical of groundmass phlogopite (Mitchell 1995), and do not show any systematic trend. The zoning also involves significant depletion in Na (Fig. 11A) and F (from 1.2–2.1 to 0–0.9 wt.%). Occasionally, SEM studies reveal patches of Ba- and Ti-poor compositions in cores of the largest phlogopite grains. Similar Ba- and Ti-poor phlogopite is found rarely in the cores of phlogopite replacing “kimberlitized” granitic xenoliths (Table 2). Further evolution of phlogopite in these areas proceeds along the typical Al-enrichment trend. However, rims of phlogopites in patches of assimilated felsic material may be overgrown by a 10 μm rim of biotite (Table 2) or by apatite. Both types of mantle are commonly in contact with serpentine and Ca-silicate containing traces of Al and Fe (epidote?), which replace granitic xenoliths.

Phlogopite compositions in sample 39–270 are much less diverse, and zoning is less pronounced (Table 2). Typically, the mica is homogeneous phlogopite close in composition to zoned rims of sample 21–K4. Rare zoned crystals exhibit gradual trends of Al enrichment and Fe, Ba and Ti depletion from core to rim, or irregular patches of low-Fe phlogopite in rims. F, Na and Ba are present in significant amounts. F content is typically constant (0.5 to 2 wt.%), but Ba and Na tend to decrease from core to rim. Interestingly, BaO correlates with TiO<sub>2</sub> (Fig. 11B), which is not observed in sample 21–K4. Major local controls on phlogopite compositions are evident in the data. Phlogopite growing after assimilated felsic material is distinctly richer in Ti and Ba. A phlogopite rim in contact with strontian apatite is uniquely poor in Ti and Ba, but a rim of another grain 10 μm away is richer in these oxides by 1 wt.%. Phlogopite rims next to pectolite and another Ca-silicate (Fig. 5E) shows abnormally high FeO contents and are completely devoid of Ba and Ti.

### *Macrocrystal diopside- and monticellite-bearing phlogopite – serpentine kimberlite*

In sample 8–K4, all phlogopite, poikilitic and non-poikilitic, is severely and complexly zoned. Oikocrysts with diopside are enriched in Cr<sub>2</sub>O<sub>3</sub> for up to 0.3 wt.%. The second episode of mica crystallization produced

tetra-ferriphlogopite overgrown on early phlogopite as 10–20 μm mantles, or formed discrete smaller crystals. Absence of intermediate values between core and rim compositions indicates the presence of two distinct generations of groundmass mica. The later TFP mica is poorer in Ti, Ba, and Na and is completely devoid of Al and F. Yet another generation of phlogopite is observed as the outermost 5 μm rims that occasionally overgrow TFP rims. They show either sharp or smooth contacts with the third-generation phlogopite. These latest phlogopite variants are poorer in FeO by 8 wt.%, in K<sub>2</sub>O by 1 wt.%, and richer in Na<sub>2</sub>O by 0.5 wt.%. The uneven development of the latest Na-rich phlogopite is controlled by its neighboring minerals. Na-rich rims crystallize near serpentine, but are absent next to pectolite (Fig. 5F), the structure of which accepts Na.

### *Macrocrystal diopside- and melilite-bearing phlogopite – serpentine kimberlite*

Sample 61–K2 features homogeneous phlogopite with between-grain heterogeneities controlled by their textural positions. Poikilitic groundmass mica is Ti- and Al-rich phlogopite, which is unusually enriched in Ti compared to other phlogopite from the 5034 hypabyssal kimberlite. It also shows a peculiar trend of well-correlated Al and Ti (Fig. 11D). A chemically distinct phlogopite is found overgrown on diopside crystals. This phlogopite has significantly lower TiO<sub>2</sub> content (as much as 5 wt.% less) and BaO (as much as 1 wt.% less), and higher FeO (up to 2 wt.% more) than the groundmass phlogopite.

### *Macrocrystal phlogopite – serpentine kimberlite*

In contrast to all other studied samples, mica in sample 11–K5D is represented by high-Al phlogopite with increased contents of eastonite and kinoshitalite. Phlogopite grains (20–100 μm) crystallize in radially oriented rosettes that are extensively replaced by chlorite. Cores of ~10% grains are barian phlogopite overgrown by a discrete generation of Ba-poor phlogopite (Fig. 5D, Table 2). Clear bimodal distribution of all elements in cores and rims of the phlogopite suggests two separate events of phlogopite crystallization. Although low-Ba phlogopite is poorer in TiO<sub>2</sub>, a single trend of Ba–Ti correlation is absent (Fig. 11G). The phlogopite of the second generation is lower in Al<sub>2</sub>O<sub>3</sub> by ~6 wt.%, and richer in FeO by ~4 wt.% and MgO by 4 wt.%.